A&A manuscript no.
(will be inserted by hand later)
Your thesaurus codes are:

ASTRONOMY AND ASTROPHYSICS
June 12, 1999

From clouds to stars

Protostellar collapse and the evolution to the pre-main sequence

G. Wuchterl[1,3] and W.M. Tscharnuter[1,2]

[1] Institut für Theoretische Astrophysik der Universität Heidelberg, Tiergartenstraße 15, D–69121 Heidelberg, Germany
[2] Interdisziplinäres Zentrum für Wissenschaftliches Rechnen der Universität Heidelberg, Im Neuenheimer Feld 368, D-69120 Heidelberg
[3] Institut für Astronomie der Universität Wien, Türkenschanzstraße 17, A-1180 Wien, Austria,

Vs.: 12. Juni 1999; Received Date; accepted date

Abstract. We present the first study of early stellar evolution with 'cloud' initial conditions utilizing a system of equations that comprises a solar model solution. All previous studies of protostellar collapse either make numerous assumptions specifically tailored for different parts of the flow and different parts of the evolution or they do not reach the pre-main sequence phase. We calculate the pre-main sequence properties of marginally gravitationally unstable, isothermal, equilibrium 'Bonnor-Ebert' spheres with an initial temperature of 10 K and masses of 0.05 to 10 $M_\odot$. The mass accretion rate is *determined* by the solution of the flow equations rather than being prescribed or neglected. Usually stellar evolution calculations start with the young star already at its final mass or with an initial stellar embryo containing only a fraction of 1 $M_\odot$ subsequently growing to its final mass with an assumed and often constant accretion rate.

In our study we determine the protostar's radii and the thermal structure together with the mass and mass accretion rate, luminosity and effective temperature during its evolution to a stellar pre-main sequence object. We calculate the time needed to accrete the final stellar masses, the corresponding mean mass accretion rates and median luminosities, and the corresponding evolutionary tracks in the Hertzsprung-Russell diagram. We derive these quantities from the gas flow resulting from cloud collapse. We do not assume a value for an 'initial' stellar radius and an 'initial' stellar thermal structure at the 'top of the track', the Hayashi-line or any other instant of the evolution. This is achieved by solving the flow equations for a cloud fragment with spherical symmetry. The system of equations we use contains the equations of stellar structure and evolution as a limiting case and has been tested by a standard solar model and by classical stellar pulsations (Wuchterl and Feuchtinger 1998, A&A, 340, Feuchtinger 1999, A&A Supl. 136 , A&A in press, Feuchtinger and Dorfi 1999, A&A, subm.).

Protostars of 2 $M_\odot$ appear close to the location of the Henyey part of the respective classical evolutionary track and at substantially larger ages for given luminosities than inferred from previous calculations. 1 $M_\odot$ stars appear at lower luminosities, to the left of the Hayashi-tracks and are about 1 Myr older. They burn most of their Deuterium during the main accretion phase before mass accretion halts and they become visible. They do not become fully convective during the entire evolution calculated, i.e., up to 1.5 Myr. Very low mass stars and proto brown dwarfs close to the substellar limit appear with luminosities close to those at the 'top of the tracks', giving ages roughly in accord with classical values, tentatively at 0.05 to 0.09 dex higher effective temperatures.

Key words: star formation, protostars, protostellar collapse, fluid dynamics, time-dependent convection, pre-main sequence evolution, Deuterium burning, stellar evolution, cloud collapse, brown dwarfs: formation

1. Introduction

Present stellar evolution theory mostly deals with stars that are in hydrostatic equilibrium, where gas pressure balances gravity. The motion and inertia of stellar gas are usually neglected. The starting point of stellar evolution calculations is the early pre-main sequence phase. One important aim of star formation theory being still an unsolved problem is to provide the initial conditions for stellar evolution, i.e., the masses, radii and the internal structure of young stars as soon as they can be considered to be in hydrostatic equilibrium for the first time[1].

[1] From these extended initial states the stars contract because energy losses from the surface are not (fully) compensated by nuclear energy generation in the deep stellar interior.

Send offprint requests to: G. Wuchterl
wuchterl@ita.uni-heidelberg.de

The calculation of appropriate starting conditions for stellar evolution is complicated by the fact that, in general, young stars still accrete mass. Therefore, the hydrostatic parts of young stars and their photospheres are more or less directly connected to circumstellar material, being in motion due to mass-inflow and/or outflow. Both moving circumstellar matter and the accretion process are by nature non-hydrostatic. Flows that contain both the hydrostatic protostellar core and the hydrodynamic accretion flow must be calculated by using at least the equations of radiation hydrodynamics including convection and cause a wealth of technical difficulties.

Modelers of early stellar evolution and the pre-main sequence phase have therefore relied on simplified concepts to make the problem tractable. Originally, Hayashi et al. (1962) argued that the cloud collapse should be so fast that the fragment would evolve adiabatically to stellar conditions and the hydrostatic young star would appear as an isentropic sphere radiating at high luminosities, thus causing a fully convective structure, close to the top of the Hayashi-track.

Larson (1969) showed that radiative losses during collapse are substantial and early collapse would proceed isothermally. Detailed models showed the necessity of a careful budgeting of the energy losses in the framework of radiation hydrodynamics (RHD) and demonstrated the high accuracy requirements for a direct calculation of the collapse (Appenzeller and Tscharnuter 1974, 1975, Bertout 1976, Tscharnuter and Winkler 1979, Winkler and Newman 1980 a,b, Tscharnuter 1987, Morfill, Tscharnuter and Völk 1985, Tscharnuter and Boss 1993, Balluch 1991a,b,c, Kürschner 1994). Modelers then looked for simplified, sometimes semi-analytical concepts to characterize the collapse and accretion flow with key parameters chosen in accord with values from detailed RHD-models of protostellar collapse or from properties of specific collapse solutions like the constant mass accretion rate for the self-similar singular isothermal sphere or those resulting from accretion disk models. (Stahler Shu and Taam 1980a,b, 1981, Stahler 1988, Palla and Stahler 1993, Lenzuni, Chernoff and Salpeter 1992, Siess et al. 1997, 1999). Another approach is the continued study of the isothermal phase (e.g., Foster and Chevalier 1993).

The various simplification strategies can be classified by the way the complete problem is split into a quasi-hydrostatic 'stellar' and a hydrodynamic 'accretion' part, both in space and in time: (1) Quasi-hydrostatic calculations use high luminosity initial conditions for a given stellar mass, i.e., with accretion assumed to have terminated or only causing negligible effects on the pre-main sequence. Once the mass is chosen, the initial entropy and radial entropy structure has to be specified before the initial model can be constructed. The choice of entropy essentially results in a value for the stellar radius. To be sure that the details of the star formation process, or more precisely, the specific initial conditions do not influence such studies, the initial luminosities are chosen to be very high. If they are sufficiently high, the later evolution rapidly becomes independent of the earlier evolution.

(2) The same procedure as above stated but for a small mass initial core (typically chosen to be $0.05\,\mathrm{M}_\odot$) that is embedded in a steady accretion flow with given mass accretion rate. The procedure is thought to reduce the ambiguity in the initial entropy structure by lowering the initial hydrostatic mass. The entropy added to the initial core is calculated self-consistently with the prescribed mass addition from the steady inflow due to disk/or spherical accretion. The lowered arbitrariness in the initial entropy structure (mass and initial entropy only have to be chosen for a small fraction of the mass and result in an initial radius for the initial hydrostatic core) is accompanied by the requirement of additionally specifying the mass accretion rate $\dot{M}$ and the state of the gas at the cloud boundary. The key advantage, however, is that, due to the assumption of the steadiness of the accretion flow, the mathematical complications are reduced considerably by changing a system of partial differential equations into one of ordinary differential equations.

(3) Parameterized mixtures of (1) and (2), see Siess et al. (1997) for a recent discussion.

Thus the theoretical knowledge about protostellar collapse and the pre-main sequence remained separated. On the one hand, modeling based on classical stellar structure theory was able to produce pre-main sequence tracks that could be related to observations if the question about the initial entropy distribution was put aside. On the other hand, models of the protostellar collapse revealed the entropy structure to be a signature of the accretion history, but were unable to provide pre-main sequence observables needed to be confronted with observations.

Recent advances, both in computational techniques and in the modeling of time-dependent convection, now make it possible to calculate the pre-main sequence evolution directly from cloud initial conditions by monitoring the protostellar collapse until mass accretion fades and the stellar photosphere becomes visible. We present the results of such calculations for cloud fragments of masses ranging from 0.05 to 10 $\mathrm{M}_\odot$ and discuss the consequences for the hydrostatic stellar evolution on the pre-main sequence.

2. Theoretical concept

Our considerations focus on the requirement for a physically motivated and well defined concept that describes the beginning of stellar evolution. Such a concept cannot

---

The stars shrink but the motion is so slow that inertia can be neglected and the stars remain close to hydrostatic equilibrium. At the end of this quasi-hydrostatic phase the energy radiated into space from the photospheres is *balanced* by nuclear energy generation. Then the stars are at the (zero age) main-sequence and in the so-called 'complete' (mechanical and thermal) equilibrium.

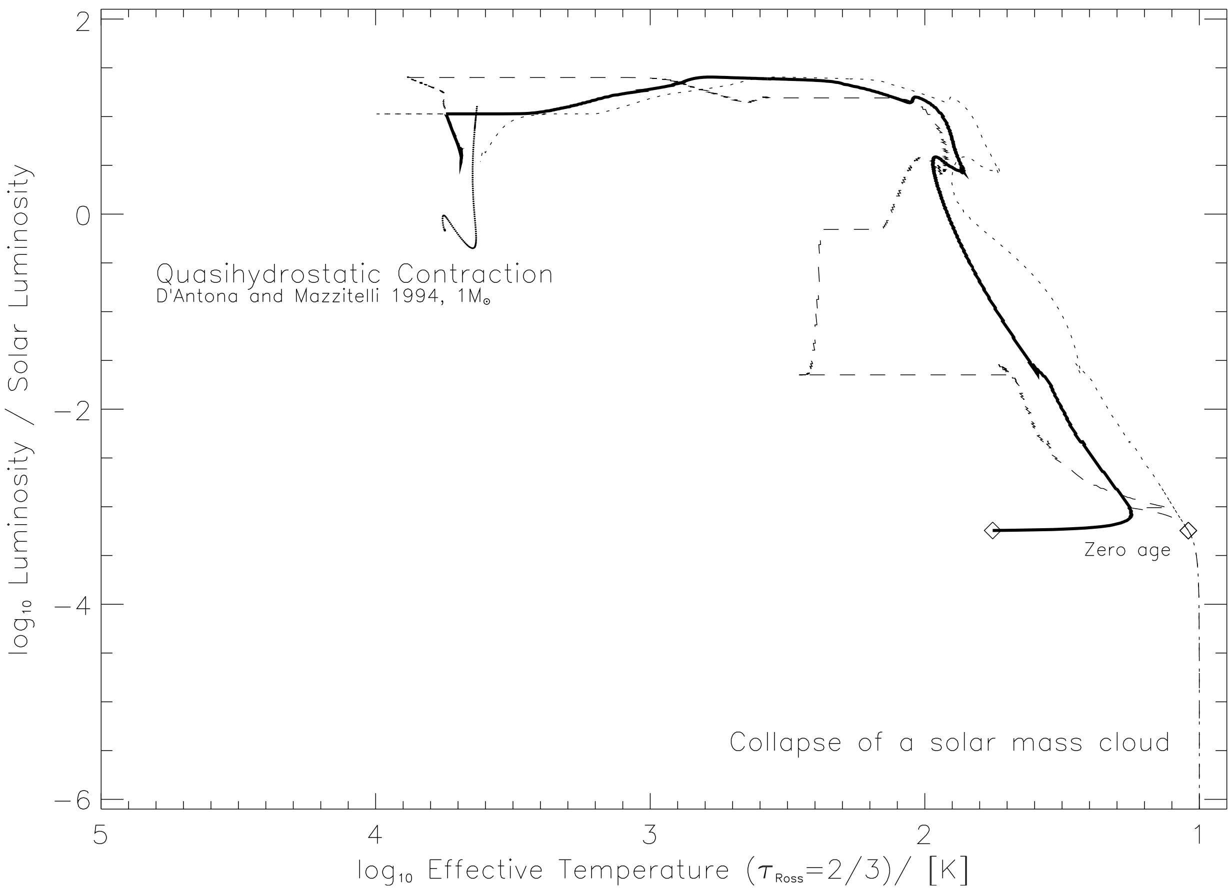

Fig. 1. Early stellar evolution in the Hertzsprung-Russell diagram: Comparison of results for the collapse of a $1\,\mathrm{M}_\odot$, 'Bonnor-Ebert' sphere (thick line) and a classical pre-main sequence track (*thin line*). Both are for mixing length convection, with $\alpha_{\mathrm{ML}} = 1.4$. The classical PMS-track (thin line on the left) is the $1\,\mathrm{M}_\odot$, 'MLT Alexander', case after D'Antona and Mazzitelli 1994. The *thick line* for the cloud collapse gives the effective temperature as defined by $L = 4\pi r_\tau^2 \sigma T_{\mathrm{eff}}^4$. r_τ is the radius at which the Rosseland mean optical depth, τ_{Ross} as integrated inward from the outer boundary of the cloud equals 2/3. Alternative temperatures are given for the cloud collapse results: The *dashed line* is the temperature defined by $L = 4\pi r^2 \sigma T^4$, at the first point encountered inward starting from the outer boundary of the cloud, i.e., based on the *temperature radius* as discussed by Baschek et al. (1991). The *dotted line* gives the temperature at $\tau_{\mathrm{Ross}} = 2/3$, an estimate for the photospheric temperature. Note that the photospheres obtained in the collapse calculations are convective at this point and $T = T_{\mathrm{eff}}$ is not guaranteed. The two diamonds indicate zero age, defined here as the moment when $\tau_{\mathrm{Ross}} = 2/3$ for the first time. Temperatures before zero age (on the dash dotted curve) are central temperatures of the still transparent cloud. The alternative temperatures are given here to illustrate the uncertainties involved in putting a collapsing cloud fragment into the HRD and to emphasize different physical aspects.

be based on *a priori* hydrostatic models. With reference to hydrostatic pre-main sequence studies Appenzeller (1982) noted:

> '... that in view of the results of the (hydrodynamic) protostellar evolutionary computations the computed hydrostatic tracks for $M > 3\mathrm{M}_\odot$ and the computed fully convective sections of all hydrostatic tracks are probably physically meaningless or (at best) rough approximations only since the initial (and boundary) conditions assumed in the computations of hydrostatic tracks are too different from those resulting from the preceding protostellar evolutionary stages.'

Therefore we evaluate the conditions at the beginning of stellar evolution as a consequence of the star formation process. We assume that the latter is determined once the properties of the initial cloud fragment are specified. We study stellar formation for a set of assumptions of the cloud state and study early stellar evolution as a consequence of the collapse of the initial conditions in the cloud. In other words, we establish a quantitative theoretical link between studies of the fragmentation process and early stellar evolution.

Since our aim is to calculate the properties of a young star before it reaches the main sequence for a given interstellar cloud fragment we have to take into account a certain minimum set of physical processes in order to calculate stellar properties on the pre-main sequence in a reliable way. In addition, we have to describe the cloud physics in sufficient detail to obtain a useful initial condition. In the sequel, we put together something like the minimum physics necessary to describe both phenomena—cloud fragments and stars—with one set of equations/assumptions.

Calculations of stellar properties require a treatment of self-gravity, the counteracting gas pressure that produces hydrostatic equilibrium, radiative and convective energy transfer in the optically thick stellar interior, a treatment of the photosphere, i.e., radiative transfer at low optical depths and nuclear energy generation.

Because there are only models for convective energy transfer—a theory based on basic principles is still lacking—we have used a twofold strategy to test the convection model and to calibrate its free parameters—the only free parameters in our set of equations. First of all the convection model has a limiting behaviour that very closely approximates mixing length theory for a set of standard values of its free parameters. As with mixing length theory (MLT) the calibration of the free parameters is done by calculating a solar model using the 'stellar structure limit' of our equations and compare it to the Sun. Secondly, the time-dependent parts of the convection model that go beyond MLT have been tested in the 'stellar hydrodynamics limit' of our equations by comparing non linear pulsations models of RR Lyrae lightcurves with observations (Wuchterl and Feuchtinger 1998, Feuchtinger 1999a,b).

Following the evolution of a collapsing cloud fragment requires self-gravity, a description of the (supersonic, compressible) motion of the cloud gas, radiative transfer in extended, non-planeparallel media of low, moderate and very high optical depth, and, sooner or later in the non-isothermal phase, a time-dependent treatment of convection.

We account for all of the mentioned processes that are of importance in clouds and stars. However, we assume spherical symmetry and the grey Eddington approximation for radiative transfer to keep the problem as simple as possible, since this is the first unified look on the problem of cloud collapse, star formation and early stellar evolution. In the next section we assemble a system of equations that contains all the physics described above.

To discuss the results and illustrate the differences we emphasize the comparison with classical, i.e., fully hydrostatic results that are obtained with model equations (stellar evolution equations) being as close as possible to the 'stellar structure limit' of our set of equations; we will not compare our results to studies that include more physical processes in one way or another. For example, we determine the mass accretion rate from our flow equations which automatically turn into our stellar structure equations when accretion fades. We do not rely on a parameterized description of mass-accretion that is invoked during phases where accretion is thought to be applicable. The advantage of our approach is that there is a known mathematical relation between our equations and the assumptions which are made in classical stellar evolution theory presently used in any case to calculate stars in their pre-main sequence phase and thereafter. Such a relation cannot be given easily and is much less clear once additional processes are added a posteriori and in a parameterized way.

For the comparison of our results to quasi-hydrostatic stellar evolution calculations on the pre-main sequence we chose the calculations by D'Antona and Mazzitelli (1994), DM94, as our reference for the following reasons:

1. The photospheric radiative transfer in DM94 is an almost[2] accurate limit of our grey radiative transfer in the Eddington approximation in its 'stellar structure limit'. We thereby exclude differences between our calculations and the quasi-hydrostatic calculations which might be due to effects that are specific to the details of the non-grey treatment of the photospheres.
2. The low temperature, molecular opacities for DM94, 'Alexander' sets of PMS-tracks are the same as used here.
3. standard mixing length convection, our 'stellar structure limit' for convection, is one of the convection theories used by DM94.

3. A model for protostellar collapse and the pre-main sequence

Because this study unifies two fields that are usually separated we first discuss how to obtain our system of equations starting with the equations usually adopted in each of the two fields, namely studies of cloud collapse and studies of the pre-main sequence evolution.

3.1. From cloud collapse to stellar evolution

Starting with the equations of cloud collapse that are valid in the isothermal phase we can obtain our system of model equations in the following way. Because we focus on the energetics here, the most important complications arise from the increasing importance of a careful treatment of energy transfer, as soon as the cloud collapse proceeds

[2] DM94 exclude convection at Rosseland mean optical depths $\tau < 2/3$ implicitly by the specific $T(\tau)$ relation they use in their photospheric model, see Chabrier and Baraffe (1997) for a more detailed discussion.

beyond the isothermal phase. It is well known that a detailed treatment of energy transfer becomes important to determine the temperature once the cloud has become optically thick. In this respect, the calculations of cloud collapse carried out by Winkler and Newman (1980a,b), Balluch (1991,a,b,c), Morfill, Tscharnuter and Völk (1985), Tscharnuter (1987), Tscharnuter and Boss (1993), and Kürschner (1994) come closest to stellar conditions. These 'non-convective' studies treat the non-isothermal, quasi-adiabatic main accretion phases and carry out detailed radiative transfer calculations in the framework of radiation hydrodynamics of supersonic accretion flows.

Results from those studies were used to check the new convective studies in the early phases where convection plays only a minor role. Early on, the results of radiative collapse calculations are not much changed by convection. A detailed discussion, including the effects on the stability of early protostellar cores, will be given elsewhere.

Balluch (1991a) discussed steady radiative accretion flows and used it as a test to check the system of equations and the method of finding a solution of the fully time dependent set of equations, in the steady limit (Balluch 1991c). Our flow equations, when neglecting convection and nuclear reactions, correspond to Balluch's (1991c), time-dependent flow equations in the Eddington approximation. Since we also use essentially the same numerical method as Balluch (1991c) (see Dorfi and Feuchtinger 1995 for a discussion of improvements) his test in the steady limit also tests our model equations and numerical methods. This is, of course, not applicable to the convection model.

There are essentially two processes that had to be added to the existing, non-convective studies of cloud collapse in order to obtain all the physics necessary at the pre-main sequence: (1) nuclear reactions and (2) convection.

Appenzeller and Tscharnuter (1974, 1975) included hydrogen burning and convection in a stellar structure type fashion by setting the radial temperature gradient equal to the isentropic (adiabatic) value in convectively unstable layers (ZEG convection). Furthermore they assumed a simplified structure for the accretion shock and used the diffusion approximation for radiative transfer. Winkler and Newman (1980a,b) discussed and improved the accuracy of these collapse calculation, especially radiative transfer but did not include convection and thermonuclear reactions.

Ondrejkovics Fernandes (1990) calculated the protostellar collapse to the formation of the inner (second) atomic hydrogen core, with the equations of RHD that are used here. She included convection by a much more elaborated time-dependent convection model than the one used here. It is an extension of the Kuhfuß model that ought to have an improved accuracy up to convective Mach numbers of ≤ 4. However, turbulence must be seeded in this model by assuming small values. Furthermore the relation of this convection model to standard models as well as its behaviour under known circumstances, especially in the Sun, remains to be investigated.

Our work may be viewed as a continuation of the studies cited above with the addition of the effects of Deuterium-burning and time-dependent convection with a known relation to mixing length theory. While the former is conceptually straightforward, the latter represents an important progress in this work. From the point of view of modeling cloud collapse it is worth mentioning that convection is an important process to be included in stellar models, especially for young stars that are born close to the Hayashi lines of fully convective models in the Hertzsprung-Russell diagram. In our collapse calculations transient convection even occurs in the first (outer) molecular hydrogen core that forms as a transient hydrostatic structure due to the opaqueness caused by the dust opacities.

Finally we note that the equations used here contain all isothermal studies of spherical cloud collapse (e.g., Hunter 1977 or, more recently Foster and Chevalier 1993) as special cases for specific initial and boundary conditions.

3.2. From stellar evolution to collapse radiation hydrodynamics

Starting with the equations of stellar structure, we must add a description of the dynamical effects of gas flow, i.e., extend the equation of hydrostatic equilibrium to the full equation of motion of fluid dynamics. This introduction of the inertia of matter into stellar evolution changes the mathematical nature of the stellar evolution calculations. The hydrodynamical equations introduce hyperbolic parts into the system of structure equations and, as a consequence, a space-time structure. Time is not any more a parameter of quasi-static models that change thermally due to energy transfer, surface losses and locally according to the laws of thermodynamics.

An immediate consequence of the rapid, non quasi-static changes during the collapse is that the stellar structure description of convection has to be extended to dynamical, i.e., in general non-hydrostatic, time dependent situations. Eddy turnover times are comparable to the local sound crossing time-scale. The required time-dependent theory of convection must also be capable to describe the onset of convection in a completely radiative flow. This is different from time-dependent convection in stellar pulsations where convective regions are only modulated by the pulsation. Modelling the onset of convection is an obvious requirement because the initial cloud state is isothermal, and certainly convectively stable everywhere, but young stars appear in the vicinity of the Hayashi lines of fully convective gas spheres. Therefore convection has to be switched on, somewhere between the isothermal cloud and the Hayashi-line, in a regime that is known to be characterised by supersonic collapse flows.

The third key addition to the stellar structure equations comes from the fact that it is necessary to perform radiative transfer in the collapsing cloud, i.e., to extend the treatment of radiative transfer to geometrically extended regions of the flow at moderate and low optical depth (the extended initial states do not behave like a compact, planeparallel stellar photosphere and require the inclusion of the effects of spherical geometry)[3]. In practice large fractions of the flow (and the mass) are nonhydrostatic and located in large, spatially extended regions at low and moderate optical depths at various times during the evolution. Clearly the flow is transparent initially and throughout the isothermal phase. Furthermore the flow is generally fully time-dependent, i.e., non-static, non-steady. It contains radiating, sometimes supercritical shocks that call for a time-dependent description of the radiation field (cf. Winkler and Newman 1980a,b). We note that our convection model also behaves physically plausible under such conditions (cf. Wuchterl and Feuchtinger 1998). The time-dependence of the radiation field is an important difference to stellar structure and most of stellar hydrodynamics (see Feuchtinger 1999a) where matter and radiation are usually assumed to be in equilibrium—an assumption used to formulate the classical set of stellar structure equations. As a consequence of this time-dependent description of the radiation field, we distinguish between two temperatures for matter and radiation, respectively, that are generally non-equal, even in the grey, i.e., frequency independent case.

3.3. Model equations

We use the equations of radiation hydrodynamics (RHD) in the grey Eddington approximation and with spherical symmetry (Castor 1972, Mihalas and Mihalas 1984) in their integral form (Winkler and Norman 1986). Convective energy transfer and mixing is included by using a new, time-dependent convection model (Wuchterl and Feuchtinger 1998) derived from the model of Kuhfuß (1987)[4]. It closely approximates standard mixing length theory in a local, static limit and has been successfully tested in calculations of the Sun and RR Lyrae pulsations (Wuchterl and Feuchtinger 1998). The convection model is used with the standard parameters given in Wuchterl and Feuchtinger (1998). The few cases where the mixing length parameter $\alpha_{\rm ML}$ is changed are explicitly emphasized. In all other cases the standard value $\alpha_{\rm ML} = 1.5$ is used, which results in a solar model that is in accord with standard solar models and the Sun for our 'stellar structure limit'. The equations and boundary conditions are summarized in Table 1, in the appendix.

Detailed equations of state (Wuchterl 1989, 1990) and opacities for a (proto) solar composition are used (X = 0.77, Y = 0.213, Z = 0.017, $X_D = 3.85\,10^{-5}$). The equations of state have been compared to the MHD equations of state (Mihalas et al. 1988) and agree to better than the table-interpolation errors (cf. Götz 1993). Opacities include the contribution of dust particles with 'interstellar' properties (Yorke 1979, 1980a), Alexander and Ferguson (1994) values in the molecular range and Weiss et al. (1990) Los Alamos high temperature opacities (compilation by Götz 1993). Convective mixing of Deuterium and Deuterium burning (with reaction rates from Caughlan and Fowler 1988) and the convective mixing of Deuterium are included as outlined in the next section.

3.4. Deuterium burning

During early stellar evolution the first nuclear reaction that contributes significantly to the energy budget of a young star is the D burning reaction ^{2}H(p, γ)^{3}He. The energy release of 5.5 MeV per reaction contributes as a source $\epsilon^{\rm D}_{\rm nuc}$ to our internal energy equation. In the volume integrated form the source term reads:

$$\int_{V(t)} \varrho \epsilon^D_{\rm nuc}\, d\tau\,, \tag{1}$$

with

$$\epsilon^D_{\rm nuc} = \frac{Q_{\rm D}}{\varrho} \tilde{r}_{^2{\rm H(p,\gamma)}^3{\rm He}}\,, \tag{2}$$

$$\tilde{r}_{^2{\rm H(p,\gamma)}^3{\rm He}} = n_{\rm p} n_{\rm D} \langle \sigma v \rangle_{^2{\rm H(p,\gamma)}^3{\rm He}} \tag{3}$$

$$= \varrho_{\rm p} \frac{N_{\rm L}}{A_{\rm p}} \varrho_{\rm D} \frac{N_{\rm L}}{A_{\rm D}} \langle \sigma v \rangle_{^2{\rm H(p,\gamma)}^3{\rm He}}\,. \tag{4}$$

The proton partial density, $\varrho_{\rm p}$, is approximated by the hydrogen partial density, Xϱ. Once D becomes significantly depleted, it has to be budgeted by the D balance equation that accounts for D destruction and transfer from regions of different D abundance due to advection and convective mixing:

$$\frac{d}{dt}\left[\int_{V(t)} \varrho_D\, d\tau\right] + \int_{\partial V} \left[\varrho_D u_{\rm rel} + j_{\rm D}\right]\cdot dS = \int_{V(t)} \dot{\varrho}_D\, d\tau \tag{5}$$

where $j_{\rm D}$ is the D flux due to convective mixing,

$$j_{\rm D} = -\alpha_{\rm M} \Lambda \sqrt{\frac{3}{2}} u_{\rm c} \varrho \frac{\partial c_{\rm D}}{\partial r}\,, \tag{6}$$

(Kuhfuß 1987), for D concentration $c_{\rm D} = \varrho_{\rm D}/\varrho$, mixing length Λ, convective velocity $u_{\rm c}$, (cf. Wuchterl 1995a,

[3] Unlike in the modeling of stellar structure it is in general not possible to separate energy transfer in the interior from the (simplified) photosphere. Concepts for fitting regions at low and high optical depths may be found for certain evolutionary phases (e.g., quasi steady flow during the main accretion phase) but processes like the *formation of a photosphere*, that is part of star formation can obviously not be described by apriori assuming the existence of the entity to be formed.

[4] The model described by Kuhfuß (1986) is very similar to the 1987 version but the latter contains a more careful discussion and treatment of the mixing-length limit of the model.

Wuchterl and Feuchtinger 1998), the unavoidable free parameter for the mixing efficiency, set to its standard value $\alpha_{\rm M} = 1/2\sqrt{2/3}$ (Kuhfuß 1987), and

$$\dot{\varrho}_D = \frac{A_{\rm D}}{N_{\rm L}} \tilde{r}_{^2{\rm H(p,\gamma)^3He}} = \frac{A_{\rm D}}{N_{\rm L} Q_{\rm D}} \varrho \epsilon^D_{\rm nuc} , \tag{7}$$

is the rate of change in D partial density due to destruction of D nuclei by nuclear reactions. Rate coefficients, $\langle\sigma v\rangle$ for ^{2}H(p, γ)^{3}He are taken from Caughlan and Fowler (1988)[5]. D burning via ^{2}H(p, γ)^{3}He is the only nuclear reaction that we take into account. As a consequence, our study is limited to evolutionary phases before the onset of Hydrogen burning and does not address the evolution of abundances of trace species like ^{7}Li and Be.

3.5. Establishing the stellar structure limit

With the generalized system of equations given in Table 1, a crucial test is that they should work in the stellar structure limit. This is assured by (1) using the equations of radiation hydrodynamics which contain the stellar structure equations and (2) the construction of a convection model with a limiting behaviour which closely approximates mixing length theory. That this is not only a formal relation but corresponds to observed stellar properties has been tested by Wuchterl and Feuchtinger (1998) in the following way: The time derivatives have been set to zero, a model of the solar convection zone has been integrated and quantities at the bottom of the convection zone have been compared to standard solar models. Other calculations such as the determination of the properties of stellar models resulting in double mode RR Lyrae pulsations put tight constraints on the accuracy of the stellar structure treatment that follows from our model equations (Feuchtinger 1998).

We rely on models of classical stellar pulsations as a test (in the nonlinear radiation hydrodynamical regime) of our equations and solving methods including especially the test of the non linear, time-dependent properties of the convection model. Those stellar pulsation models, with the system of equations that we use here for star formation studies, result in RR Lyrae (colour) lightcurves that are in detailed accord with observations (Wuchterl and Feuchtinger 1998, Feuchtinger 1999b, Feuchtinger and Dorfi 1999). In particular nonlinear RR Lyrae models calculated with our convection model resolve the ‘Fourier phase discrepancy problem’ (Feuchtinger 1999b) and successfully model double mode pulsation behaviour of RR Lyrae (Feuchtinger 1998).

The calculations are also a test for the adopted standard values of the free parameters of the convection model that we consider to be fixed in this application to star formation.

[5] GW thanks H. Herndl for providing a subroutine for the calculation of D reaction rates.

To summarize, the aforementioned studies show that the system of equations and the employed methods of finding a solution work correctly for physical reference systems in the ‘stellar structure’ limit of those equations and the non linear, radiation-hydrodynamic regime of stellar pulsations (RR Lyrae stars).

In this respect it is assured that our extensions to the system of stellar structure equations do have a fixed relation to standard stellar structure and stellar hydrodynamics. After this procedure the model equations we use do not contain any additional free parameters and the formation and evolution of a star is determined by the properties of the initial cloud fragment alone. The star formation theory is fully specified with the specification of the initial cloud state and the boundary conditions.

4. Numerical techniques and improvements

The equations are solved with a ‘protostellar’ version of the VIP-code (Dorfi and Feuchtinger 1995), where convection is added as outlined by Wuchterl (1995a). The equations are discretized following the principles described by Winkler and Norman (1986) and Tscharnuter (1987, 1989) with a tensor pseudo viscosity (Tscharnuter and Winkler 1979) and a self-adaptive grid determined by an equation of the Dorfi and Drury (1987) class. For a recent comparative discussion of discretisation techniques see LeVeque (1998) and for an overview over the self-adaptive grid method see Tscharnuter (1991) and Dorfi (1998).

The VIP code contains improvements with respect to other self-adaptive grid codes used to calculate the protostellar collapse. The most important one being a higher order (van Leer) advection scheme (see Dorfi and Feuchtinger 1995)[6]. The key advantage in the present context is that a higher order advection scheme allows the grid to move faster, for a given advection error. Hence grid points can be concentrated more rapidly and higher spatial resolution can be obtained faster. The advection errors caused by local grid refinement are an important ‘side effect’ of using an adaptive grid when very high resolution is obtained on timescales that are much smaller than the physical timescales in the flow (Kürschner 1994). This side effect is only present when the flow is non steady

[6] The advantages of using higher order advection schemes in adaptive mesh radiation hydrodynamics have been demonstrated by Winkler and Norman (1986). ‘Radiative’ protostellar collapse has been calculated earlier by using second order advection methods in the WH80s code. Those calculations did use a different grid equation (Winkler and Norman 1986). The VIP code is the first radiation hydrodynamics code that combines more accurate advection schemes with the much clearer grid equation by Dorfi and Drury (1987). The VIP code is in many aspects related to the Titan code (Gehmeyr and Mihalas 1993), that is the offspring of the Winkler WH80s code (see Mihalas 1998). All those codes are based on implicit numerical methods using a self-adaptive grid.

and, as a consequence, the motion of the gridpoints contributes to the advection errors.

For our calculations of the protostellar collapse, modifications of the VIP-code have been made. They can be understood as a consequence of the quantitative resolution requirements and accuracy demands of a protostellar collapse calculation. Many of these requirements have been discussed previously (Tscharnuter and Winkler 1979, Tscharnuter 1987, Morfill et al. 1985, Balluch 1991a,b,c, Kürschner 1994). We will briefly describe the modifications as motivated by a view based on the properties of self-gravitating equilibrium gas spheres (with radiation) as they are imposed onto those systems by their gravity. This emphasizes the accuracy requirements that become increasingly important toward the end of the star formation process. Increasing fractions of the cloud fragment mass actually settle into hydrostatic equilibrium as the pre-main sequence is approached. Earlier high resolution studies focused on the accurate representation of the flow discontinuities (e.g., Balluch 1991a,b,c) because the hydrostatic parts were relatively easy to resolve with a self-adaptive grid. Nevertheless, they deserve a careful consideration because they contain a large fraction of the total mass. After all, that fraction should approach unity at the end of a star formation calculation.

4.1. Spatial resolution

A hydrostatic sphere of gas with given temperature, be it a cloud fragment, a star, a brown dwarf or a giant planet, has a typical 'pressure' scale height,

$$H_P = -\frac{P}{g\varrho} = \frac{c_{\mathrm{T}}^2}{g} \sim \frac{e}{g}\,, \tag{8}$$

where pressure, P, gravitational acceleration, g, and density, ϱ usually vary both in space and time (see Baschek et al. 1991 for a general formulation). c_{T} and e are the isothermal sound speed and the internal energy per unit mass. This mechanical structure is imposed by gravity directly via the force balance of the hydrostatic equilibrium, independent of the details that lead to the specific pressure and density or sound speed in the gas sphere. If the pressure is high the influence of gravity is relatively weak. High pressure systems with small gravity almost behave non-gravitating, with no radial gradients in thermodynamic equilibrium. In our context of star formation the typical example for such a weakly gravitating equilibrium system is the marginally stable isothermal cloud fragment. Length scales below a Jeans wavelength,

$$\lambda_{\mathrm{Jeans}} = \frac{\pi c_{\mathrm{T}}^2}{G\varrho}\,, \tag{9}$$

are stabilized by gas pressure. A marginally stable cloud with radius λ_{Jeans} has a minimum pressure scale height of

$$H_P^{\mathrm{Jeans}} = \frac{c_{\mathrm{T}}}{\sqrt{\frac{16}{9}\pi^3 G\varrho}} \sim c_{\mathrm{T}}\tau_{\mathrm{ff}}\,. \tag{10}$$

If we compare the Jeans scale height to the Jeans length we obtain a ratio of the length scale over which the pressure changes relative to the overall cloud size, i.e.,

$$\frac{H_P^{\mathrm{Jeans}}}{\lambda_{\mathrm{Jeans}}} = \frac{3}{4\pi^2} \sim 0.1\,. \tag{11}$$

In other words, a Jeans critical cloud is quasi-homogeneous, with pressure changes within an order of magnitude[7].

At the end of a star formation calculation gravity becomes much more important for the overall structure, especially in the outermost layers of the stars, where temperature and pressures are smallest. After all, the dominating effect of gravity is the key reason of why spherical symmetry is a good approximation through most parts of stellar evolution. For the Sun we obtain a ratio of the photospheric pressure scale height to the solar radius, of

$$\left.\frac{H_P}{R}\right|_{\odot} \sim 2\,10^{-4}\,. \tag{14}$$

For a star formation calculation this means that, as the cloud collapses, gravity is becoming more and more dominating and the scale heights are becoming correspondingly smaller. In general the respective dimensionless number to specify the relative length scale over which flow variables vary in a gravitating system close to hydrostatic equilibrium is given by the *compactness*,

$$\frac{r}{H_P} = \frac{r_{\mathrm{acc}}}{r} = \frac{GM}{rc_{\mathrm{T}}^2} \sim 5000\left(\frac{c_{\mathrm{T},\odot}^2}{c_{\mathrm{T}}^2}\right)\left(\frac{\mathrm{R}_\odot}{r}\right)\left(\frac{M}{\mathrm{M}_\odot}\right) \tag{15}$$

the meaning becoming more obvious with the r_{acc} expression. $c_{\mathrm{T},\odot}^2$ is the isothermal sound speed for solar effective temperature. In any numerical calculation the local pressure scale height has to be resolved by a few 'zones'. This translates into a numerical resolution requirement estimating the length scales which are introduced by gravity alone, i.e., when all dynamical effects are neglected (e.g., no ram pressure, no shocks, etc.). Traditionally this has been met by using the pressure as a coordinate and discretizing in $\log P$, but this is only possible with the strictly monotonic pressure $P(r)$ produced by hydrostatic equilibrium. That approach cannot be used in hydrodynamical

[7] We can estimate the mean mass accretion rate for star formation from such a cloud by

$$\dot{M}_{\mathrm{Jeans}} = \frac{M_{\mathrm{Jeans}}}{\tau_{\mathrm{dyn,Jeans}}} \quad \text{with} \quad \tau_{\mathrm{dyn,Jeans}} = \frac{\lambda_{\mathrm{Jeans}}}{c_{\mathrm{T}}} \tag{12}$$

and obtain

$$\dot{M}_{\mathrm{Jeans}} = \frac{4\pi^2}{3}\frac{c_{\mathrm{T}}^3}{G} \sim \frac{c_{\mathrm{T}}^3}{G}\,, \tag{13}$$

which is a valid estimate as long as the mean cloud densities are close to those of equilibrium configurations (singular or regular) and the temperature, and as a consequence the sound speed, c_{T}, does not change. For our cloud assumptions we obtain $\dot{M}_{\mathrm{Jeans}} = 2.3\,10^{-5}\mathrm{M}_\odot/\mathrm{yr}$.

studies because pressure cannot be used as a global coordinate.

When hydrostatic parts *and* a circumstellar gas flow are calculated together, as is the case in our study, the compactness directly translates into a lower limit for the required local radial resolution (Wuchterl 1995a):

$$\frac{r}{\Delta r} > \frac{r}{H_P}\,. \tag{16}$$

Any calculation of the forming Sun has to resolve the outer stellar layers with at least the respective local refinement of $\sim 10^4$. To make progress on an evolutionary timescale the timestep should be at least on the global dynamical timescale R/c_s with $\Delta r/r = 10^{-4}$ and hence the numerical scheme must be able to cope with Courant numbers of 10^4 to at least study global dynamical phenomena. To follow the evolution on the Kelvin-Helmholtz time-scale,

$$\tau_{\mathrm{KH},\odot} = \frac{G\mathrm{M}_\odot^2}{\mathrm{R}_\odot \mathrm{L}_\odot} \sim 30\,\mathrm{Myr}\,, \tag{17}$$

of thermal contraction—which is typically 10 orders of magnitude larger than the dynamical time-scale for the Sun—the numerical scheme has to progress at Courant numbers of the order of 10^{14}. Hence any scheme that can provide the necessary resolution has to be implicit.

A hydrodynamic calculation that does not satisfy the resolution requirement (16) cannot distinguish between a dynamic pressure gradient caused, e.g., by a sound wave and the hydrostatic 'background' structure! In practice there is, of course, much more flow structure to be resolved on a pressure scale height. Radiative transfer, e.g., requires a resolution in optical depth that sometimes is much more stringent as it requires $\Delta\tau < 0.01$ (cf. Balluch 1991a)[8]. The condition (16) above and the resulting Courant numbers therefore must be viewed as a demanding but still relatively weak lower limit. In practice resolutions of $r/\Delta r \sim 10^{10}$ are needed towards the end of the calculations presented here.

The compactness is a dimensionless number that can be used to quantify both the effects of gravity and the respective resolution requirements in astrophysical radiation hydrodynamics. It can also be used to distinguish between systems with different importance of gravity effects (Wuchterl 1995a). The analogy to the square of the Mach number describing the importance of inertial effects is displayed below:

$$\mathrm{Mach}^2 = \frac{u^2}{c^2} \sim \frac{e_\mathrm{kin}}{e_\mathrm{therm}} \qquad \frac{r_\mathrm{acc}}{r} = \frac{GM}{rc_\mathrm{T}^2} \sim \frac{e_\mathrm{grav}}{e_\mathrm{therm}}\,. \tag{18}$$

The collapse flow leading to the formation of a $1\,\mathrm{M}_\odot$ star, for instance, involves Mach numbers up to 400 and a compactness of 10^4. For comparison: Accretion flows on proto giant planets are much easier to calculate because Mach number and compactness involved are both around 10 (cf. Wuchterl 1995b). RR Lyrae and δ Cephei stars have compactness between a few 100 and 1000 and the Mach numbers for the pulsation-flows are around 10. White dwarfs have compactness ranging from $5\,10^4$ to $2.5\,10^5$; neutron stars finally approach maximum compactness, $c^2/2c_\mathrm{T}^2$ with radii of a few Schwarzschild radii, $R_\mathrm{S} = 2GM/c^2$.

4.2. Advection

For a calculation of protostellar collapse the condition (16) means that, from the equilibrium structure of gravitating systems alone, we have to resolve at least structures starting from 0.1 to 10^{-4} of the local radius. The latter is about 10^{-10} of the extension of the computational domain, the initial volume of the cloud fragment. In practice this is needed to describe the 'background' structure on top of which the radiation hydrodynamics of the collapse proceeds. In principle, the required resolutions are no problem for a self-adaptive grid method and we could solve the Navier-Stokes equations with the 'molecular' viscosity and omitting any pseudo viscosity as demonstrated by Balluch (1991c). But this pushes present computer floating point operations to its limits (quadruple precision is then needed and slows down the computations considerably), and the 'realistic' molecular viscosity might cause large advection errors during time-dependent flow phases. To meet the resolution requirements of gravitating equilibrium systems while keeping the advection errors as small as possible we use a pseudo viscosity length scale, l_visc, defined by

$$\frac{1}{l_\mathrm{visc}} = \frac{1}{\alpha_\mathrm{visc}}\left(\frac{1}{r} + \frac{1}{H_P}\right)\,. \tag{19}$$

The harmonic mean with r assures that the length-scale for pseudo viscosity is specified in units of the local radius in weak gravity parts of the flow. Calculations presented here are made for $\alpha_\mathrm{visc} = 0.01$, comparison calculations to check the non-dependence of the results on this computational parameter have been made for values down to 10^{-4}. The pseudo viscosity is a numerical tool that is used to calculate viscous dissipation in shocks on length scales larger than those of the molecular mean free path, where it would occur naturally. The resolution requirements for the numerical solving method are relaxed by the corresponding increase in pseudo viscosity relative to molecular viscosity. Of course, it would be satisfactory to adopt the 'realistic' values for molecular viscosity and start out with the Navier-Stokes equations directly, but the resolution requirements are very high $r/\Delta r \sim 10^{11}$ (Tscharnuter 1991), even very early in the collapse after first (outer) core formation. The consequences of such high resolution are either very high grid point numbers or advection errors during time-dependent phases, when a self-adaptive grid is used. Both the high resolution and the high advec-

[8] The optical depth scale height is equal to the pressure scale height in classical, compact static photospheres (Baschek et al. 1991), hence the τ refinement translates into a H_p-refinement.

tion speeds cause an additional computational effort. To avoid this we use the above $l_{\rm visc}$ to obtain a compromise between high resolution, large grid point numbers, large advection speeds and large floating point accuracy. With our choice of computational parameters it is assured that shock dissipation takes place on length scales that are two orders of magnitude smaller than the natural length scales of gravitating equilibria. If shocks appear our flow model starts to become viscous on that small relative scale. This avoids the 'mixing of scales' and has the advantage that calculations can be carried out using only double precision (14–16 digit) floating point operations and makes it possible to calculate the collapse with only 1000 grid points. As the compactness of the forming star increases our maximum resolution gradually increases and advection errors are kept to the necessary minimum.

The previous considerations guarantee that the spatial resolution is sufficiently high but low enough to avoid unnecessary advection errors when high resolution is required fast. In other words, grid induced advection is avoided by considering the sources for grid motion during time-dependent evolutionary phases. We also improved the advection scheme by demanding *volume conservation*, i.e.,

$$\frac{d}{dt}\left[\int_{V(t)} d\tau\right] + \int_{\partial V} u_{\rm grid}\cdot dS = 0 \tag{20}$$

to be satisfied algebraically by the advection scheme. This demand results in an expression for $u_{\rm rel}$, the velocity of the grid relative to the flow

$$u_{\rm rel} = u - u_{\rm grid} = u - \frac{1}{3}\frac{\delta r^3}{r^2\delta t} = u - \frac{1}{3}\frac{1}{\delta t}\left(r - \frac{(r^*)^3}{r^2}\right) \tag{21}$$

to be used in the discretisation of the advection terms (see Dorfi 1998 for a geometric discussion). We use advection fluxes calculated from the various densities and velocities in all equations rather than using the temporal change in interior mass (as advocated by Winkler and Norman 1986 and used in the standard version of the VIP-code, cf. Dorfi and Feuchtinger 1995). The calculation of the advection terms from the velocities results in a slightly modified discretisation of the equation of motion (no spatial averaging in the momentum densities). As a consequence of this modification of the advection scheme the advection errors reported by Kürschner (1994), which produce step-like features when grid speeds are very high become negligible even for grids that are similar to the grids he used.

4.3. Hydrostatic parts and total energy

To improve total energy conservation we use the freedom that is available in formulating the grid equations after Dorfi and Drury (1987). First we limit the grid speed by a time-constant for the grid

$$\tau_{\rm grid} = g_\tau\left[t_{\rm ff}\left(\frac{M}{4\pi r^3}\right) + 1000\right][s]\,, \tag{22}$$

where $t_{\rm ff}(\varrho)$ is the free-fall time for the enclosed mass, i.e., we specify the time constant for the grid in units of the free-fall time corresponding to the local mean density of the gravitating mass. The weighting factor g_τ is set 100 to assure that the relative Mach numbers of the grid remain below ~ 100 everywhere. This reduces the total energy errors due to advection that have been identified (Kürschner 1994) to significantly contribute to the oscillation amplitudes found for first protostellar cores.

Secondly, to enhance the resolution in hydrostatic parts of the flow that carry large fractions of the total energy (and total energy errors, cf. Kürschner 1994) we weight the arc-length in our desired resolution function (sometimes also called the monitor function) for the grid equation motivated by a scaled estimate for the total potential energy content of the respective mass shell,

$$g_l = \tanh\left(\frac{r^2 M_r}{{R^*}^2 M^*} - 1\right) + 1\,, \tag{23}$$

$$R_{\rm grid} = \Phi_{\rm grid} = \sqrt{1 + \sum_x g_l g_x \left(\frac{Df}{Dr}\right)^2}\,, \tag{24}$$

where Df,Dr: $Dx = \Delta x/\bar{x}$ are the usual, harmonically scaled differences of the flow variables ($f \in \{\kappa, \rho, s, T, \nabla_{\rm s}\}$) in the VIP code that enter the desired resolution. Gradients in places with large $E_{\rm grav}$ are strongly weighted in the arc-length for the desired resolution function. For the weights in the resolution function we use $g_x = 0.3$ for the results shown, and used g_x-values down to 0.01 in comparison calculations.

Our general method to distinguish between different candidate prescriptions for the 'arbitrary' or 'personally biased' part of the Dorfi and Drury (1987) grid equation was to use the total energy conservation properties as a criterion. A better grid is considered to be one that conserves total energy better. By this approach the freedom in specifying the desired resolution function has been somewhat reduced compared to other studies.

4.4. Discretization Remarks

The discretisation of the nuclear energy generation source term to the internal energy equation is done analogously to other source terms. The D balance equation is discretized in analogy to the continuity equation. We note that we use D concentration as our additional computational variable and that we use a discretization for $j_{\rm D}$ which is symmetric in the grid index.

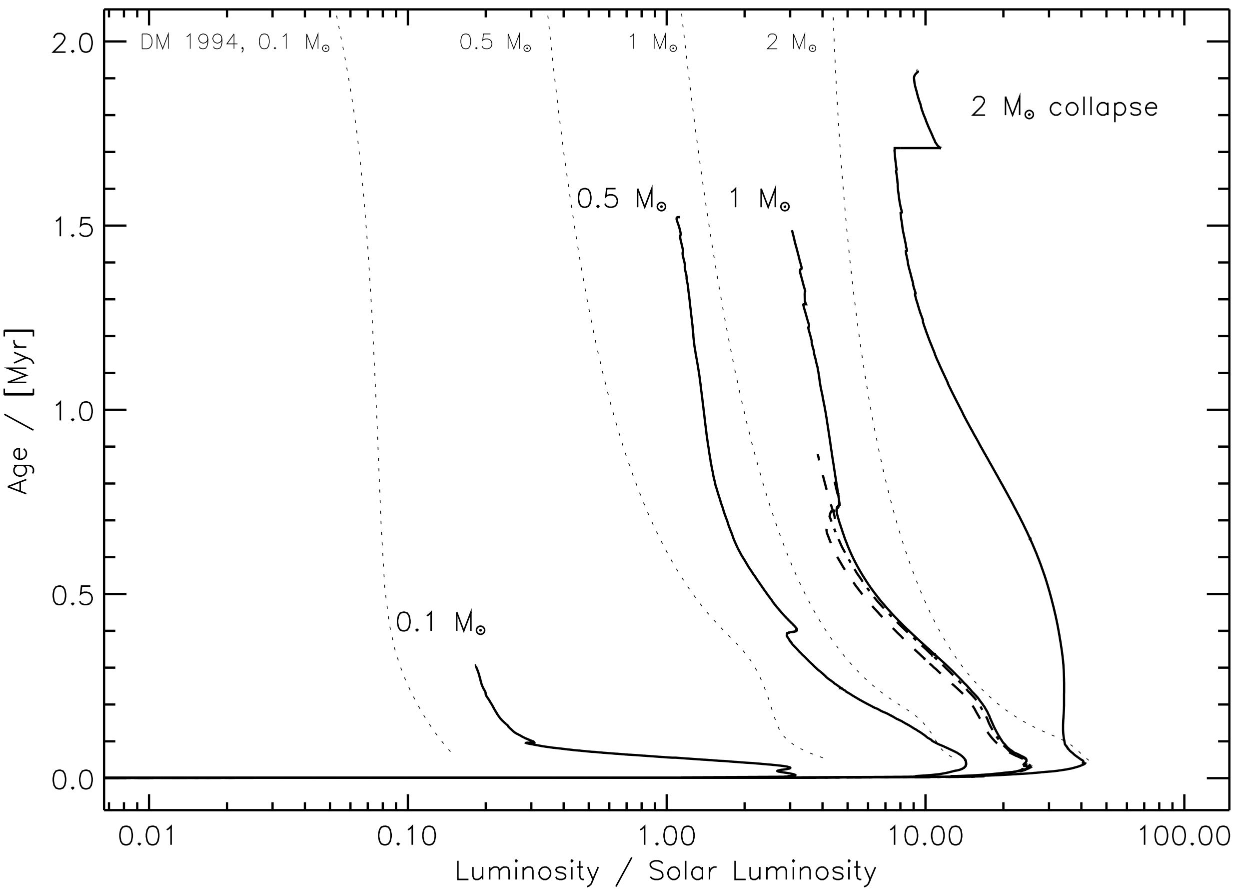

Fig. 2. The relation between age and luminosity for the collapse of Bonnor-Ebert spheres (*full lines*) and classical, fully hydrostatic models of pre-main sequence evolution. These relations are relevant for the determination of PMS-ages. For the comparison we use the quasi-hydrostatic results by D'Antona and Mazzitelli (1994) ('Alexander + MLT' case) for $0.1, 0.5, 1$ and $2\,\mathrm{M}_{\odot}$ (*dotted lines* from left to right). Classical PMS-models do not accrete and evolve at constant mass. The new PMS-ages calculated from the collapse of cloud fragments are larger than the classical values by up to a Myr, depending on luminosity. This is due to an age offset because the formation process is modeled and due to a different PMS-contraction behaviour caused by the difference between the assumed initial thermal structure in classical tracks and the thermal structure calculated from the collapse and accretion process. Note that collapse luminosities show an initial rise, close to zero age, as the protostars are 'switched' on after core formation. Ages inferred using collapse PMS-tracks will be larger than those inferred from classical tracks by up to a Myr at ages below 2 Myr. The *dashed* and *dash-dotted line*, close to the $1\,\mathrm{M}_{\odot}$-relation, are obtained by changing the mixing length parameter α_{ML} to 1.2 and 1.4, respectively, for the same fragment mass, see text.

5. Collapse of Bonnor-Ebert spheres

In this section we discuss the results for the collapse of critical Bonnor-Ebert spheres with a temperature of $10\,\mathrm{K}$ and masses of 0.05 to $10\,\mathrm{M}_{\odot}$ within a constant volume, as obtained by the methods described above.

5.1. Constructing the initial conditions

The critical, i.e., marginally gravitationally unstable Bonnor-Ebert sphere was determined numerically in the following way: We started with a homogeneous, isothermal sphere of one tenth of the Jeans-critical density. After dynamical relaxation this sphere becomes hydrostatic and quasi-homogeneous with only a weak central density enhancement. The calculations are carried out for a given volume (originally, the volume corresponding to 0.1 of the Jeans density) that is slowly contracted (at $\dot{R} = 0.01\,\mathrm{cm\,s^{-1}}$). The subcritical hydrostatic sphere therefore shrinks on the time-scale $R/\dot{R}$, which is $\sim 10^{19}\mathrm{s} \sim 320\,\mathrm{Gyr}$. The calculations (with the fully dynamic equations) proceed on this time-scale through a sequence of essentially static isothermal spheres, $L \sim 10^{-10}\,\mathrm{L}_{\odot}$ until the marginally stable equilibrium sphere is reached and collapse sets in. This procedure guarantees that the initial cloud condition is accurately static and that the critical state for the detailed constitutive relations (most prominently the pressure equation of state) is determined precisely.

5.2. Structure of results and definitions

The results described below are quantities derived from the flows which are obtained as the solution for the Bonnor-Ebert collapses. Since there is no a priori hydrostatic part and no a priori photospheric model in our model (they result as special properties of the solutions of our flow equations) we briefly describe how the stellar parameters age, effective temperature, radii and masses are obtained from the radiation hydrodynamical flows. We restrict our discussion mostly to these basic parameters to give an overview over the collapse solutions. We start our discussion with a proposal for the definition of zero stellar age, because as it turns out, most our definitions of stellar parameters will only be valid after this instant of time.

5.3. Stellar zero age

The modeling of the star formation process together with the PMS-contraction opens up the possibility to define a stellar zero age. We require the instant of age zero to be

1. well defined,
2. a unique clock for an individual star; it should be reset by a destruction of the star and stellar mergers, and
3. the gravitationally weakly bound, tenuous states of the cloud should not contribute to stellar age — a long lasting quasi static cloud phase would otherwise induce almost arbitrary age additions without any consequences for the subsequent evolution.

To compare the luminosities of objects of various masses at a given age a general definition of zero age is necessary. As the thermally controlled Kelvin-Helmholtz contraction is the dominating evolutionary process in young gas spheres, whether they are giant planets, brown dwarfs or stars, we propose, to use the instant of time, when the interior of the gas spheres is thermally enclosed for the first time, as age zero. The enclosure means that photons cannot escape from the entire object directly but are radiated from a photosphere. Energy transfer to the photospheric bottleneck then delays the cooling and determines how the thermal reservoir in the interior is emptied. The cooling history can then be used to define an age since the heat reservoir was formed. As a practical definition for age zero we propose to use the instant of time when the Rosseland mean optical depth of a gaseous object equals 2/3, i.e.,

$$\mathrm{Age} = 0 : \tau_{\mathrm{Ross}}(t) = \int_{r'}^{R} \kappa_{\mathrm{Ross}} \varrho \, dr = \frac{2}{3} \,. \qquad (25)$$

We use 2/3 here because of the advantage for, e.g., the T_{eff} definition in the comparison to D'Antona and Mazzitelli (1994) but recommend to use Age $= 0$ at $\tau_{\mathrm{Ross}}(t) = 1$, in general. $\tau = 2/3$ results from an averaging of optical depth over the stellar disk that is specific to the grey Eddington approximation.

For a protostar this instant of time is practically at the end of the isothermal phase of the collapse. Furthermore, with definition (25) the luminosities of the protoplanets can be compared to stars and brown dwarfs of similar age. The proposed definition of zero age has the following properties:

1. it preceeds the short phase of the 'final hydrostatic core formation' for protostars that was used in earlier work (Appenzeller and Tscharnuter 1975, Winkler and Newman 1980a) by only $\sim 2000\,$yr. It corresponds to the sharp initial luminosity rise (within 1000 yr for 0.05 to 10 $\mathrm{M}_\odot$) that occurs when the first (molecular hydrogen) protostellar cores form. Because this happens during this rapid dynamical density enhancement due to early cloud collapse, the proposed definition is very sharp, in the sense that the properties of the cloud vary rapidly in the vicinity of zero age; Age $= 0$ is reached during a phase of rapid changes in the observables. As a consequence it will be observationally well defined;
2. it is 'close' to the formation time of the oldest 'rocks' in the solar system. They presumably form during the process of planetesimal formation that occurs according to present understanding within $\sim 10^4\,$yr after pre-planetary nebula formation. The pre-planetary nebula forms roughly at the time when the final hydrostatic protostellar core settles into hydrostatic equilibrium (Tscharnuter 1987). Hence, together with the $\sim 2000\,$yr for final core formation, the ages of the oldest meteorites that are determined by absolute radioactive dating should be only $\sim 10^4\,$yr smaller than the ages defined here. This results in a conceptual consistency of our ages and the meteoritic ages to within probably $< 10^5\,$yr. It is a useful property because solar system ages of 4.566 ± 0.002 Gyr (Allègre et al. 1995, for Allende CAIs) are used to calibrate stellar structure theory by assuming that the age of the Sun is equal to the age of the meteorites and a comparison of stellar-evolution models of the Sun at theoretical ages with properties of the present Sun;
3. relative ages of different objects in a star formation region are physically well defined;
4. the thermal clock which is based on the dominating dynamical process in early stellar evolution, namely gravitational contraction and cooling is (re)set at the proposed zero age;
5. the age spread in young clusters is conceptually accessible without reference to the ZAMS, and knowledge about it. Concepts involving the ZAMS rely on the assumption that it will be reached. This is not guaranteed as it does not exist for brown dwarfs and planets. Hence such concepts would be inapplicable for those

objects. Our proposed zero age is a well defined concept for all masses at least from an earth mass up to the largest stellar masses;

6. questions about coevolution of very young binaries can be addressed because individual component ages are well defined;
7. with this zero age we use the earliest instant when an effective temperature can be defined, based on a radius defined by using optical depth.

With age definition (25) we can study the luminosity emitted by our cloud volume as a function of age. In the beginning the luminosity comes from the still almost isothermal cloud fragment, in the end from the pre-main sequence star that has formed in the centre. We will use this age to discuss the effect of the cloud collapse on pre-main sequence ages. We can expect two main effects: (i) an age offset that is due to the fact that the collapse phase which is not modeled in fully hydrostatic PMS-studies adds contributions of the order of a free-fall time to the ages usually given (see Tables 1, 2), and (ii) an effect due to the different PMS-contraction behaviour that is due to the difference between the assumed initial thermal structure of classical PMS-calculations and the thermal structure as calculated from the collapse and accretion process in this work.

In our discussion, we use the relation between luminosity and age for two reasons: (1) because of the uncertainties (both theoretical an observational) in the determination of the effective temperature of objects in the vicinity of the Hayashi-tracks, and (2) because these tracks are very steep in the HRD during the early PMS evolution — the luminosity decreases at almost constant effective temperature. These relations for the collapse of Bonnor-Ebert spheres of 0.1, 0.5 ,1 and $2\,\mathrm{M}_\odot$ are depicted in Fig. 2. The relations determined from collapse (full lines) originate from zero luminosity, i.e., before the cloud fragment starts to radiate significantly. The fully hydrostatic relations (dotted lines) begin at an assumed initial age and at a luminosity that is the consequence of the assumed (usually fully convective, or $n = 3/2$ polytrope) initial thermal structure.

Notice the age offset of about 10^5yr, about a free-fall time, between the beginning of the classical and collapse curves in all cases. This is due to the assumed initial ages of fully hydrostatic calculations. Next we look at the possibility of attributing all the differences to an age offset. This could be done by shifting the classical curves, upward to higher ages until the luminosities match the new curves. Such a procedure could be considered successful if the rates of change in luminosity of classical and collapse $L(t)$-relations match, too. This would be indicated by the luminosity difference between corresponding old and new relations of the same mass to be constant. For the $0.1\,\mathrm{M}_\odot$ case this is fairly successful and the collapse may be essentially viewed as producing an age offset of about 300 kyr. For the other masses this procedure does not hold. Even for the $0.5\,\mathrm{M}_\odot$ relations an addition of 400 kyr to the classical relation might just bring the luminosities in accord, but the relations still diverge because of the different contraction behaviour.

The consequences for the inferred ages at given luminosity are already considerable for $0.5\,\mathrm{M}_\odot$: at the end of the collapse calculation, a PMS-object with solar luminosity has a new age of 1.5 Myr while following down the $1\,\mathrm{L}_\odot$-ordinate to the classical tracks gives 0.5 Myr. The situation is very similar for the 1 and $2\,\mathrm{M}_\odot$ clouds, but the differences in luminosity evolution to the classical relations are even more pronounced. Changing the mixing length, a procedure that probably produces the largest changes in classical models does not significantly change this conclusion. This can be seen by comparing the dashed and dash-dotted lines, for $\alpha_{\mathrm{ML}} = 1.2$ and 1.4, respectively, that are very closeto the standard $M_\odot$ collapse relation.

Next the adopted age definition allows us to define the 'stellar' properties, i.e., the properties of the optically thick, ultimately hydrostatic parts of the flow for any instant after zero age. This is described in the next section.

5.4. Radii

Here we focus on the observables of the collapsing cloud fragments and the resulting young stars, so we define our stellar radii to be the optical depth radii, R_τ, obtained by determining the radius r' at which

$$\tau = \int_{r'}^{R} \kappa_{\mathrm{Ross}}\,\varrho\,dr = 2/3\,. \tag{26}$$

Because of our definition of zero age such a radius exists. This is not necessarily close to the density radius, R_ϱ, i.e., the location of the maximum absolute value of the density gradient, that usually defines the stellar radius (density gradients in shocks are ignored for this procedure cf. Winkler and Newman 1980a,b, Baschek et al. 1991). Note that Balluch (1991a,b,c) used the shock radius as an estimate for R_ϱ and the stellar radius, which is a good estimate due to the small stand-off distance of the shock.

The optical depth radius gives a measure of the radius from which the photons escape and which parts of the flow are thermally shielded from the outside. It is the length scale a (bolometric) observer would see. It is very close to the density radius once the protostellar cocoon has been sufficiently diluted by accretion to make it transparent down to the stellar photosphere. The two radii converge when R_τ 'jumps' from the dust photosphere to the stellar photosphere and intercepts R_ϱ.

5.5. Luminosity and effective temperature

With the luminosity at the outer boundary and the optical depth radius we determine an effective temperature, by

$$L = 4\pi R_\tau^2 \sigma T_{\mathrm{eff}}^4\,. \tag{27}$$

These are the $T_{\rm eff}$-values plotted in the Hertzsprung Russell diagram. To give an estimate for the uncertainty involved when placing a protostar into the Hertzsprung-Russell diagram we additionally plot two alternative temperature definitions in Figs. 1, 6, and 7: (1) a temperature $T(R_T)$based on the temperature radius, R_T, that is governed by

$$r = R_T : L(r) = 4\pi r^2 \sigma T(r)^4 \,, \tag{28}$$

cf. Baschek et al. (1991). This is the temperature at a distinct point in the flow where the luminosity corresponds to the value that would be obtained by a blackbody radiating at the local flow matter-temperature. (2) a photospheric temperature defined by

$$T_{\rm phot} = T(R_\tau) \,, \tag{29}$$

i.e., the local flow temperature at the optical depth radius. It is a measure of the temperature at the location from which the photons typically escape towards an observer.

In a static, compact, radiative photosphere in Eddington approximation, the definitions result in the same temperatures (cf. Baschek et al. 1991).

5.6. Collapse of a solar mass

The resulting theoretical Hertzsprung-Russell diagram for the collapse of a $1\,{\rm M}_\odot$ Bonnor-Ebert sphere is shown in Fig. 1. In this case the mixing length parameter $\alpha_{\rm ML}$ is chosen to be 1.4 to facilitate the comparison with the fully hydrostatic pre-main sequence calculation. The thick line shows the evolutionary track in the Hertzsprung-Russell diagram by using the effective temperature based on the optical depth radius R_τ (as used in earlier collapse studies by Appenzeller and Tscharnuter 1975 and Winkler and Newman 1980a). The track starts at the instant of zero age, indicated by the diamond symbol. As above noted the adopted definition of zero age coincides with the first instant at which the effective temperature concept can be used.

The initial decrease in $T_{\rm eff}$ is due to the fact that by definition R_τ starts out very small but rapidly increases during the first core formation. This occurs because the core's density and optical depth increase rapidly during this settling into hydrostatic equilibrium. R_τ increases at approximately constant luminosity and hence $T_{\rm eff}$ drops. Temperatures given before zero age (dash-dotted part) are central temperatures of the still transparent, almost isothermal cloud. With the onset of accretion onto the core the luminosity rises sharply with a moderate increase in $T_{\rm eff}$. The 'mouse-head' is the hall mark of the formation of the second (inner) atomic hydrogen core that forms after the (second) collapse of the dissociating molecular hydrogen core. At the cusp after the first luminosity maximum the final accretion phase is entered. As the luminosity rises towards the second maximum, the first core is accreted onto the second one and the Mach numbers of the flow increase above ten. The small luminosity decrease after the second maximum accompanies the adjustment of the accretion flow and the mass accretion rate onto the final core to the substantial luminosity now radiated from the accretion shock.

When the luminosity starts rising again the quasi-steady main-accretion phase commences. Shortly after the flat top part of the track is reached the luminosity, due to D burning, becomes significant and reaches a maximum of 60% at the global luminosity maximum. When the volume is significantly depleted by the accretion process the luminosity starts decreasing and $T_{\rm eff}$ rises as parts of the flow closer to the young star become visible. When the dust cocoon becomes transparent the optical depth radius 'jumps' into the 'stellar' photosphere the effective temperature sharply increases, crosses the classical PMS-track, the Hayashi line and finally reaches the 'corner' of the collapse track, at maximum $T_{\rm eff}$. From this point on $T_{\rm eff}$ coincides with the temperature definition based on the temperature radius (thick and dashed line overlap).

Hence the radiation hydrodynamical results for temperature based on R_T and R_τ converge to the equality valid in classical, hydrostatic photospheres. The photospheric temperature (dotted) at $\tau = 2/3$, passes the shock at this instant and produces a sharp spike to the left as $\tau = 2/3$ is at the peak temperature just downstream from the accretion shock, and still upstream from the radiative relaxation layer. As the accretion luminosity becomes negligibly small and after 'D burnout' the collapse track turns almost parallel to the classical track, slightly pointing towards the ZAMS location of the Sun on the classical track. The photospheric temperature remains different from the other two temperatures, and slightly cooler than the $T_{\rm eff}$ value of the fully hydrostatic classical track. Note that the photosphere of the collapse calculation is convective all along the Hayashi-part of the track and $T_{\rm phot} = T_{\rm eff}$, valid for a compact, hydrostatic, radiative photosphere in Eddington approximation is not guaranteed under these conditions.

5.7. Collapse PMS-tracks and isochrones

Keeping in mind the above discussion concerning temperatures we now proceed to a discussion of evolutionary tracks for cloud fragments of various masses and the respective isochrones in the Hertzsprung-Russell diagram, based on the effective temperature with the optical depth-radius definition (see Baschek et al. 1991 for a discussion, including the protostellar application). In Fig. 3 an overview over the collapse and PMS evolution of Bonnor-Ebert-sphere cloud fragments with masses of 0.05, 0.1, 0.5, 1, 2 and $10\,{\rm M}_\odot$ is given. They are compared to classical, non accreting, fully hydrostatic tracks for 0.1, 0.5, 1, and $2\,{\rm M}_\odot$ after D'Antona and Mazzitelli (1994). For the comparison an electronic version of their 'Alexander, MLT'-tracks for $\alpha_{\rm ML} = 1.4$ was used.

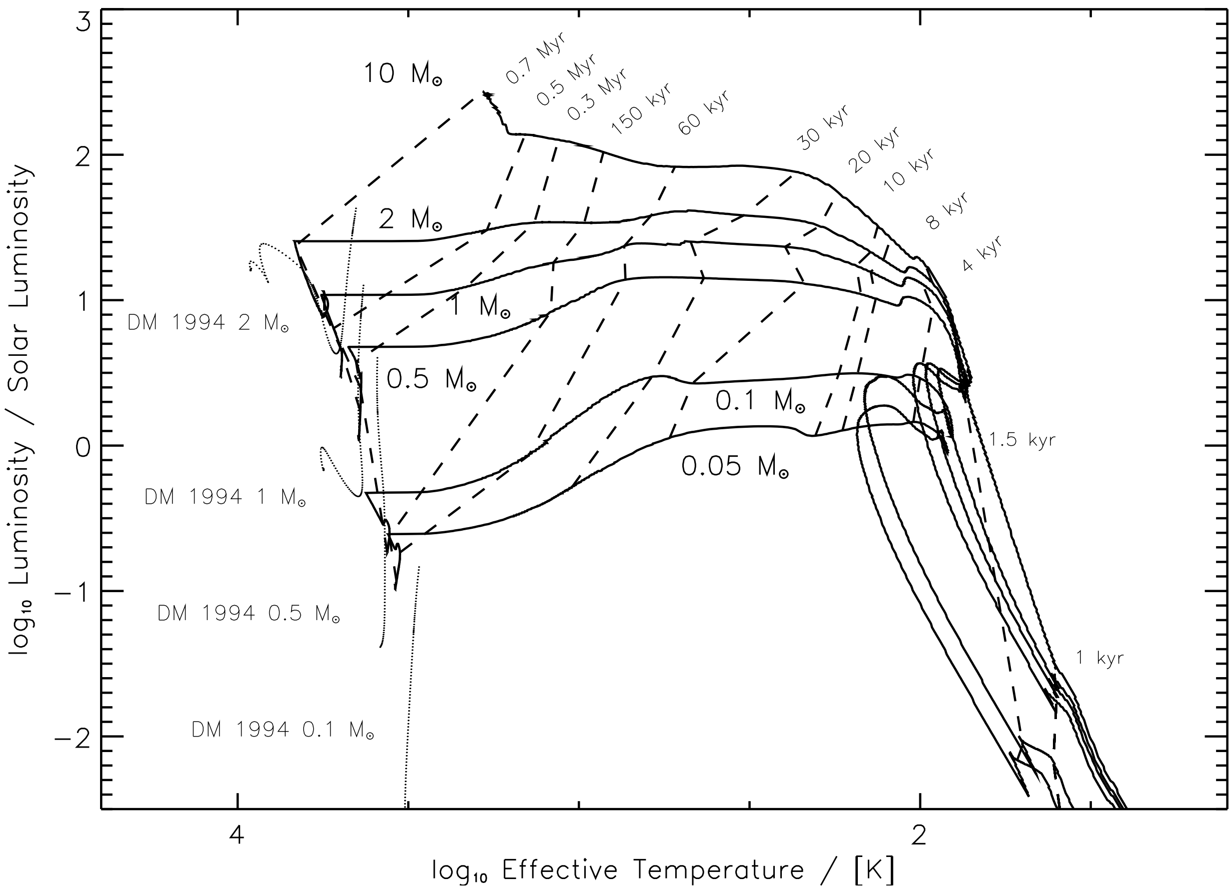

Fig. 3. Evolutionary tracks in the Hertzsprung-Russell diagram for the collapse and early pre-main sequence evolution of 0.05, 0.1, 0.5, 1, 2 and 10 $M_\odot$ cloud fragments (*full lines*). The *dashed lines* indicate isochrones for the collapse tracks, labeled with the respective ages. Zero age is defined here as the moment when the respective cloud fragment becomes optically thick and the interior is thermally locked as the first photosphere forms (Rosseland mean optical depth reaches 2/3). Quasi-hydrostatic tracks for $0.1, 0.5, 1$ and $2\,M_\odot$ from D'Antona and Mazzitelli (1994), 'Alexander MLT'-case, $\alpha_{\rm ML} = 1.4$ (*dotted lines*) are plotted for comparison.

The early evolution dominated by the initial cloud collapse is very similar for all masses. At an age of 1000 yr the first hydrostatic cores form, with an age spread of a few hundred years. All fragments enter the main accretion phase at an age slightly above 8 kyr. All tracks remain below effective temperatures of 2000 K up to 30 kyr. The protostars still remain in their dust cocoons and radiate from dust photospheres. The luminosity decline has already started at this age for the lowest mass fragment. At 60 kyr the first object has arrived on the pre-main sequence, close to the Hayashi track. It has formed from the lowest mass cloud fragment of $0.05\,M_\odot$ and is a young brown dwarf. The higher mass fragments follow until the $2M_\odot$ fragment arrives on its PMS-track at 0.5 Myr. The $10\,M_\odot$ fragment is still accreting at 0.7 Myr, with a hydrostatic central stellar embryo of $4.5\,M_\odot$.

Fig. 3 nicely illustrates that star formation is a gravitational heating event that increases temperature by about two orders of magnitude. Due to the negative, so-called gravothermal specific heat of self-gravitating systems the heating slows down when energy losses slow-down because matter becomes opaque due to the cross-sections of atoms. Ultimately nuclear energy is added which acts as a long-term thermostatic effect.

A detailed comparison with the classical tracks (dotted line) during the later phases can be made using the magnification in Fig. 4. The displayed part of the HRD essentially covers the evolutionary phases after the final stellar photospheres become visible. The horizontal parts of the collapse tracks are due to the sharp rise in effective temperature when the dust cocoon becomes optically thin and the photons start to escape directly from the stellar photosphere below the fading accretion shock. In general the collapse tracks appear about 0.05 to 0.09 dex hotter on the pre-main sequence than the classical tracks. Of course the difference depends on the luminosity but

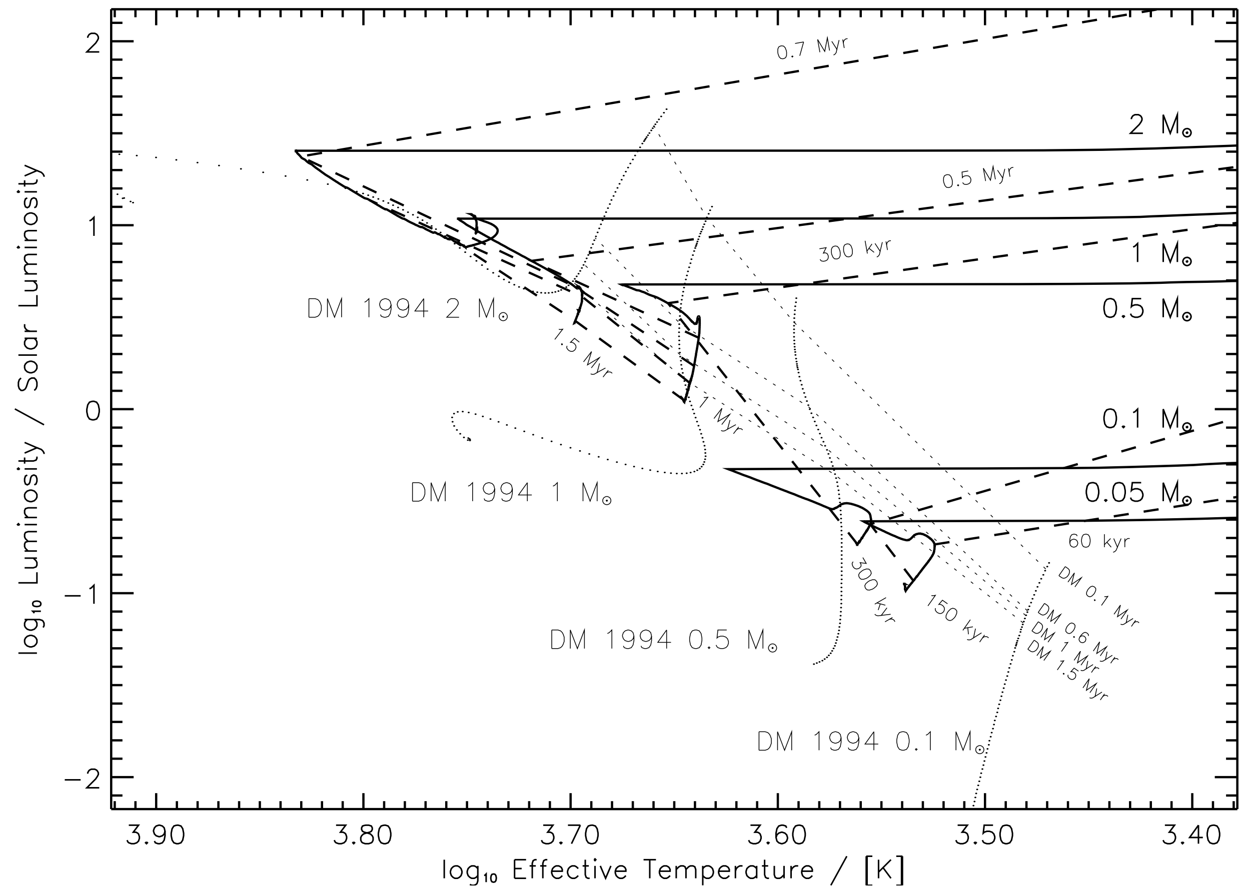

Fig. 4. Hertzsprung-Russell diagram for the early pre-main sequence evolution of 0.05, 0.1, 0.5, 1 and 2 $M_\odot$ cloud fragments (*full lines*), detail of Fig 3. The *dashed* lines are isochrones for the collapse tracks, labelled with the respective ages. Zero age is defined here as the moment when the respective cloud fragment becomes optically thick and the interior thermally locked as the first photosphere forms (Rosseland mean optical depth reaches 2/3). Quasi-hydrostatic tracks for 0.1, 0.5, 1 and 2$M_\odot$, (*dotted tracks*) and the corresponding isochrones for 0.1, 0.6, 1 and 1.5 Myr, (*dotted lines labelled with ages*) (D'Antona and Mazzitelli 1994, 'Alexander + MLT'-case, $\alpha_{\rm ML} = 1.4$) are shown for comparison. Note that, e.g., 0.5 $M_\odot$ at 1 Myr (collapse) corresponds to 1 $M_\odot$ at 1.5 Myr (classical).

the value quoted above is relevant when both tracks are roughly parallel to the Hayashi lines. The differences are not due to differences in opacities, the convection theory or the treatment of frequency dependent radiation transfer. This is assured by careful selection of the hydrostatic comparison-tracks. The accretion luminosity produced by the shock does not contribute significantly to this difference once the tracks are nearly vertical. We think that the primary reason for the increased $T_{\rm eff}$, at given luminosity is the different thermal structure with an off-centre peak-temperature, that results in more compact objects.

The early PMS evolution of the collapsed cloud fragments shows a relation to the classical tracks that change with mass. The 2 $M_\odot$ fragment arrives close to the radiative, Henyey part of the corresponding classical track. The 1 $M_\odot$ and the 0.5 $M_\odot$ case arrive on the PMS with a luminosity corresponding to about half way down on the convective, Hayashi parts of the classical tracks. The 0.1 $M_\odot$ fragment arrives with a luminosity corresponding to the top of the classical track. The 0.05 $M_\odot$ fragment (a proto brown dwarf) is shown to give an indication of the further mass dependence of the relation to the 0.1 $M_\odot$ classical track. For the two lowest masses the age difference can be attributed to an offset in zero age. Furthermore, D burning has not begun for the 0.1 $M_\odot$ case—as might be expected so close to the brown dwarf limit. It follows that, by using the appropriate initial thermal structure, this mass probably will show a quasi-classical PMS evolution starting near the top of a Hayashi track and a somewhat higher effective temperature, but, as found in previous studies, with the slow-down of contraction due to D burning.

On the other hand the results of the collapse calculations indicate substantial corrections in PMS stellar properties for masses of 0.5 $M_\odot$ and higher. PMS objects of these masses already are half-way in the direction of the Henyey-track when they become visible.

5.8. *Lines of constant mass—isopleths*

Due to our radiation hydrodynamical approach only the masses of the cloud fragments are prescribed. The stellar mass and the corresponding mass accretion rate are calculated from the flow. Hence, quantities like stellar mass and mass accretion rate are *determined* during the evolution of the flow.

For our discussion it is useful to use the optically thick mass, M_τ, for further considerations. It follows naturally by determining the mass inside the optical depth radius, R_τ that we have already used in the definition of $T_{\rm eff}$. This corresponds to the hydrostatic mass, defined, e.g., via the density radius (cf. Baschek et al. 1991) for most of the time but has to be distinguished during the very early accretion when calculating the accretion-luminosity from $GM_*/R_*\dot{M}_*$. We use M_τ for the remainder.

In order to show the stellar properties as accretion proceeds we display lines of constant optically thick mass, M_τ—which we may call *isopleths*[9]— in the Hertzsprung-Russell diagram in Fig. 5. It is the actual stellar mass that determines the stellar properties and not the fragment mass that includes the entire circumstellar environment under consideration. The $10\,{\rm M}_\odot$ fragment, for example, starts as the other fragments with $M_\tau = 0.04\,{\rm M}_\odot$ and produces the corresponding luminosities and effective temperatures despite of its $10\,{\rm M}_\odot$ protostellar envelope. The lowest isopleth at $0.01\,{\rm M}_\odot$ illustrates the fact that hydrostatic structures of that mass become optically thick (opacity limit of fragmentation) and, as a consequence, all initial protostellar cores typically form with a few percent of a solar mass. At $M_\tau = 0.04\,{\rm M}_\odot$ the lowest mass fragment has almost terminated its main accretion phase while the higher mass fragments still grow their cores and accelerate their accretion flows. As M_τ increases to the final mass the isopleths become tangential to the evolutionary tracks and at constant mass the two curves are identical. Note the decrease in luminosity when the track of a fragment approaches an isopleth close to its final mass. The beginning exhaustion of the mass reservoir becomes then noticeable as a drop in accretion luminosity. To indicate the end of significant mass accretion, the point at which 99% of the final mass has been accreted is indicated by a thin line. For the two smallest masses this happens well before they reach the Hayashi phase. Accretion, as a consequence, does not play a role *during* their PMS-contraction as calculated here. However accretion does play a role in defining their thermal structure at the 'top of the track'. For masses from $0.5\,{\rm M}_\odot$ upward the end of significant mass accretion is terminated after the Hayashi line has been crossed.

[9] From the greek words τὸ πλῆθος and ισοπλῆθής meaning 'mass' or 'crowd' and 'being of the same amount of mass', respectively.

6. Global Results

To facilitate statistical comparison with observations of star formation and to have values for the factors of order unity in scaling arguments we give some quantities averaged over the star formation time for each fragment in Tables 1 and 2. Ages at $M_\tau(t) = 0.99\,M_{\rm final}$, $t_{0.99{\rm M}}$ are given in units of Myr and the initial free-fall time; mean mass-accretion rates $<\dot{M}>= M_\tau(t)/Age(t)$ are given in ${\rm M}_\odot$/yr and $M\,M_{\rm final}/t_{\rm ff}$; M_0 is the fragment mass. For the luminosities the median values $<L>$ are given in solar units. Quantities are averaged over a time starting at zero age and ending at the end of significant mass-accretion. The end of significant mass accretion is defined as the instant at which 99% of the final mass has been accreted, more precisely when $M_\tau = 0.99\,M_{\rm final}$, cf. the respective thin line in Fig. 5. To indicate the sensitivity on the definition of the end of accretion we give a few averages obtained for the $1\,{\rm M}_\odot$ case for periods ending with M_τ closer to the final mass in Table 2.

Accretion time duration and averages

M_0	$t_{0.99{\rm M}}$		$<\dot{M}>$		$<L>$	Remark
${\rm M}_\odot$	Myr	$t_{\rm ff}$	${\rm M}_\odot$/yr	$M/t_{\rm ff}$	${\rm L}_\odot$	
1	0.55	3.23	$1.79\,10^{-6}$	0.30	13.1	RC1M
1	0.60	3.54	$1.65\,10^{-6}$	0.28	14.1	RCML15
1	0.55	3.26	$1.79\,10^{-6}$	0.30	12.8	RCML14 $\alpha_{\rm ML} = 1.4$
1	0.54	3.18	$1.84\,10^{-6}$	0.31	11.9	RCML12 $\alpha_{\rm ML} = 1.2$
0.05	0.038	4.51	$1.30\,10^{-6}$	0.22	1.02	RC005M
0.1	0.074	4.34	$1.35\,10^{-6}$	0.23	2.21	RC01M
0.5	0.32	3.81	$1.56\,10^{-6}$	0.26	7.58	RC05M
1	0.55	3.23	$1.79\,10^{-6}$	0.30	13.0	RC1M
2	1.28	3.64	$1.54\,10^{-6}$	0.27	25.1	RC2M

Table 1. Duration of accretion and averages of accretion rates and luminosities for the accretion time lasting from zero age to the end of significant mass accretion. For the end of significant mass accretion we use the moment when the young star has reached an optically thick mass M_τ of 99% of its final mass. The different $1\,{\rm M}_\odot$ cases are for different mixing length parameters.

To indicate the effects due to the time-dependence of the accretion flow, and in particular, due to the temporal variation of $\dot{M}$, we split the star formation time into 4 phases, based on $M_\tau/M_{\rm final}$. By this procedure we obtain 4 different populations corresponding to different stages of the accretion process. For each of the 4 phases we give averaged quantities, for fragment masses, M_0, of $0.05, 0.1, 0.5, 1$ and $2\,{\rm M}_\odot$, in Table 3.

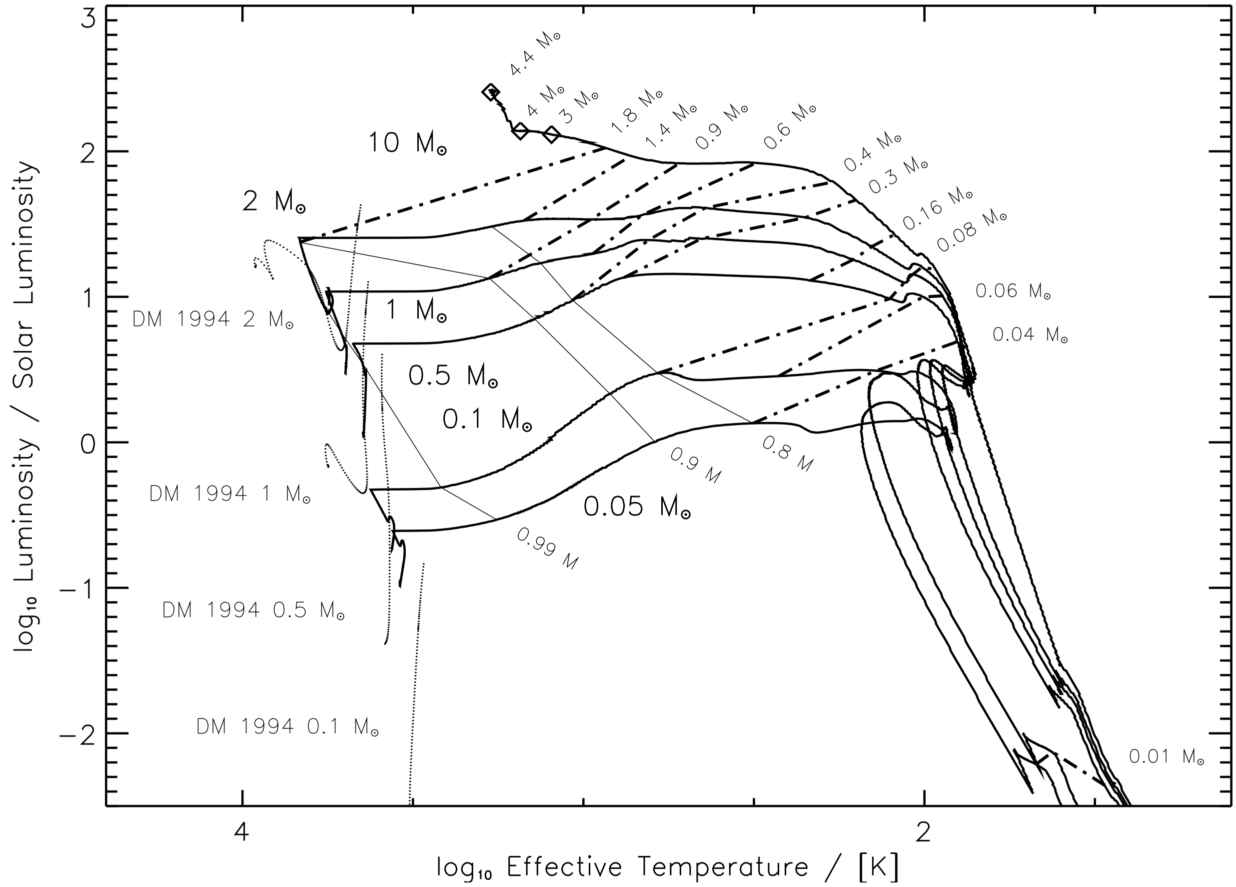

Fig. 5. Optically thick mass, M_τ, in the Hertzsprung-Russell diagram for the collapse and early pre-main sequence evolution of 0.1, 0.5, 1, 2 and $10\,\mathrm{M}_\odot$ cloud fragments. M_τ is the mass interior to the optical depth radius, R_τ. Dash-dotted lines are locations of constant M_τ, *isopleths*, with values labelled along the $10\,\mathrm{M}_\odot$-track. The locations where M_τ corresponds to 80, 90 and 99% of the final mass are connected by the *thin lines.* The thin line for 99% is used as an estimate for the end of significant mass accretion. The lines of constant mass are essentially tangential to the tracks beyond this point. Quasi-hydrostatic tracks for $0.1, 0.5, 1$ and $2\,\mathrm{M}_\odot$. (D'Antona and Mazzitelli (1994), 'Alexander MLT'-case, $\alpha_{\mathrm{ML}} = 1.4$) are shown for comparison.

Accretion time and averages for different end of accretion and a $10\,\mathrm{M}_\odot$ fragment.

M_τ $\mathrm{M}_\odot$	Age Myr	$<\dot{M}>$ $\mathrm{M}_\odot$/yr	M_0 $\mathrm{M}_\odot$	M_{final} $\mathrm{M}_\odot$	Remark
0.99	0.60	$1.67\,10^{-6}$	1	1	RCML15
0.99	0.55	$1.80\,10^{-6}$	1	1	RC1M
0.999	0.82	$1.22\,10^{-6}$	1	1	RC1M
0.9999	1.08	$9.26\,10^{-7}$	1	1	RC1M
0.99999	1.29	$7.78\,10^{-7}$	1	1	RC1M
	0.70	$7.11\,10^{-7}$	10	4.46	RC10M

Table 2. Duration of accretion and averages of accretion rates and luminosities for the accretion time lasting from zero age to the end of significant mass accretion. For the end of significant mass accretion we use different fractions $M_\tau/M_{\mathrm{final}}$ to show how averages change for the $1\,\mathrm{M}_\odot$ case. The mean mass accretion rate for the $10\,\mathrm{M}_\odot$ fragment corresponds to $0.89M/t_{\mathrm{ff}}$ in the first 0.7 Myr ($\sim 0.4\,t_{\mathrm{ff}}$)

7. A synopsis of solar mass star formation

7.1. Comparison of collapse calculations

We finally compare the existing nonisothermal studies of the protostellar collapse that reached the pre-main sequence in Fig. 6. As a magnification of Fig. 1, it shows the fully hydrostatic the one solar mass track (thin line) of DM94 and the corresponding Bonnor-Ebert collapse tracks, for the three temperature definitions as in Fig. 1 (the thick line is for T_{eff}). Both calculations use mixing length convection with $\alpha_{\mathrm{ML}} = 1.4$ in the stellar structure limit and produce solar models in accord with standard solar models.

The calculation of Appenzeller and Tscharnuter (1975) (dash-dotted line) is for zero entropy gradient (ZEG) convection and with the diffusion approximation used for radiative transfer (data from Appenzeller 1982). The differences to the present work, related to the low temperature

Averages for 4 accretion phases separated by $M_\tau/M_{\rm final} = 0, 0.8, 0.9, 0.99$ and 0.999 (cf. Figs. 5,8).

M_0		$0.05\,{\rm M}_\odot$			$0.1\,{\rm M}_\odot$			$0.5\,{\rm M}_\odot$			$1\,{\rm M}_\odot$			$2\,{\rm M}_\odot$		
	M_τ	Δt	$<\dot{M}>$	$<L>$	Δt	$<\dot{M}>$	$<L>$	Δt	$<\dot{M}>$	$<L>$	Δt	$<\dot{M}>$	$<L>$	Δt	$<\dot{M}>$	$<L>$
	$[M_{\rm final}]$	kyr	${\rm M}_\odot$/yr	${\rm L}_\odot$	kyr	${\rm M}_\odot$/yr	${\rm L}_\odot$	kyr	${\rm M}_\odot$/yr	${\rm L}_\odot$	kyr	${\rm M}_\odot$/yr	${\rm L}_\odot$	kyr	${\rm M}_\odot$/yr	${\rm L}_\odot$
0	≤ 0.8	16	$2.5\,10^{-6}$	1.28	30	$2.7\,10^{-6}$	2.92	126	$3.2\,10^{-6}$	12.4	189	$4.2\,10^{-6}$	19.5	496	$3.2\,10^{-6}$	34.1
I	$(0.8, 0.9]$	6	$8.1\,10^{-7}$	1.19	11	$8.8\,10^{-7}$	2.63	52	$9.8\,10^{-7}$	8.21	85	$1.2\,10^{-6}$	15.3	200	$1.0\,10^{-6}$	27.3
II	$(0.9, 0.99]$	16	$2.7\,10^{-7}$	0.51	32	$2.7\,10^{-7}$	0.97	144	$3.0\,10^{-7}$	4.60	280	$3.2\,10^{-7}$	8.22	592	$3.0\,10^{-7}$	13.9
III	$(0.99, 0.999]$	15	$2.9\,10^{-8}$	0.21	28	$3.0\,10^{-8}$	0.33	139	$3.2\,10^{-8}$	3.03	264	$3.4\,10^{-8}$	4.69	554	$3.3\,10^{-8}$	8.42

Table 3. Duration and averages of accretion rates and luminosities for different accretion phases of cloud fragments of $0.05, 0.1, 0.5, 1$ and $2\,{\rm M}_\odot$. The phases are defined by ranges in optical thick mass M_τ in units of the final mass $M_{\rm final}$, in the second column. For each phase and fragment mass, M_0, duration, $\Delta t = \min({\rm Age}) - \max({\rm Age})$, mean mass-accretion rates, $<\dot{M}>= \min(M_\tau) - \max(M_\tau)/\Delta t$, and the median value for the luminosities, $<L>$,is given.

phase with the initial luminosity rise, are not significant and probably largely due to the fact that the effects of the dust cocoon have been neglected by Appenzeller and Tscharnuter in the $T_{\rm eff}$ determination because of the uncertainties involved in the dust properties. The lower peak luminosity obtained by Appenzeller and Tscharnuter has been discussed in detail by Winkler and Newman (1980a) and is due to the treatment of radiative transfer and the reduced numerical resolution. It is interesting to note that the Appenzeller and Tscharnuter (1975) track coincides with the photospheric temperature track (dotted line) of the Bonnor-Ebert collapse calculated in this work. This can be attributed to the fact that the luminosities at the instant when the young star starts to radiate from the final stellar photosphere are in good agreement. But the following contraction behaviour along the Hayashi line is different for the Appenzeller and Tscharnuter (1975) track. This is probably a combined effect of the difference in the convection treatment, (ZEG in the 1975-track), the use of an ideal gas equation of state and the neglection of D burning. However, the Appenzeller and Tscharnuter track shows a similar inclination relative to the fully hydrostatic DM94-track, which may be tentatively attributed to the fact that the internal thermal structure has been calculated from the collapse flow as in this work. Differences in radiative transfer should become of negligible importance towards the lower end of all collapse tracks because the young star behavior is described by the stellar structure equations (to which Appenzeller and Tscharnuter are close) with rapidly increasing accuracy. The location of the Appenzeller and Tscharnuter track to the right of the DM94 track does not necessarily mean that it is also to the right of the *respective* Hayashi line. The appropriate Hayashi line would be the one calculated for ZEG convection, and is certainly to the right of the DM94-Hayashi part that is obtained with MLT.

The radiative collapse track from Winkler and Newman (1980a) (dash-triple-dotted line) with the data read off from their HRD shows a very good qualitative agreement with our work, which is more visible by direct inspection of their original figure in the early phases. It is important to note that Winkler and Newman (1980a) did not include convection and Deuterium burning. The increased peak luminosities (about 0.1 dex higher than here) can be fully accounted for by a radiative comparison calculation done with our model equations and convection and nuclear reactions set to zero. Hence the effects of convection are more important in this case than the improvement in radiative transfer obtained by determining the Eddington-factor from the static radiative transfer equation as done by Winkler and Newman. The lower luminosities in our study are somewhat compensated by D burning that contributes 60% of the total luminosity at the global luminosity maximum of the convective Bonnor-Ebert collapse (bump around $\log_{10} T = 2.8$ in the full line). The luminosity of the new calculation is affected by D burning above the 10% level up to $\log_{10} T = 3.4$. The much hotter temperatures and the higher luminosities obtained by Winkler and Newman once the stellar photosphere has become visible at their effective temperature maximum can be understood as a consequence of their neglect of convection. The fully radiative hydrostatic parts have much steeper gradients in convectively unstable regions. If convection were present in those regions it would act as an efficient limiter for the local temperature gradient and keep it close to the (lower) adiabatic value. Hence their objects are overall hotter and more compact. Differences in the equation of state do not play a role in this case as detailed tables have been used by Winkler and Newman that closely correspond to our equations of state, as checked in detail. Due to the smaller stellar radii matter accretes into a deeper potential and the luminosities produced by the accretion shock are higher. As the accretion ceases this effect should decrease (as is visible by comparison with the lowest part of our track) but the higher temperature due to the higher compactness that results in a smaller radiating surface remains.

To summarize, our $1\,{\rm M}_\odot$ track is placed about halfway between the radiative Winkler and Newman track and the ZEG-track by Appenzeller and Tscharnuter. Note that the evolution along the radiative Winkler and Newman track moves in the opposite direction of a classical Henyey track.

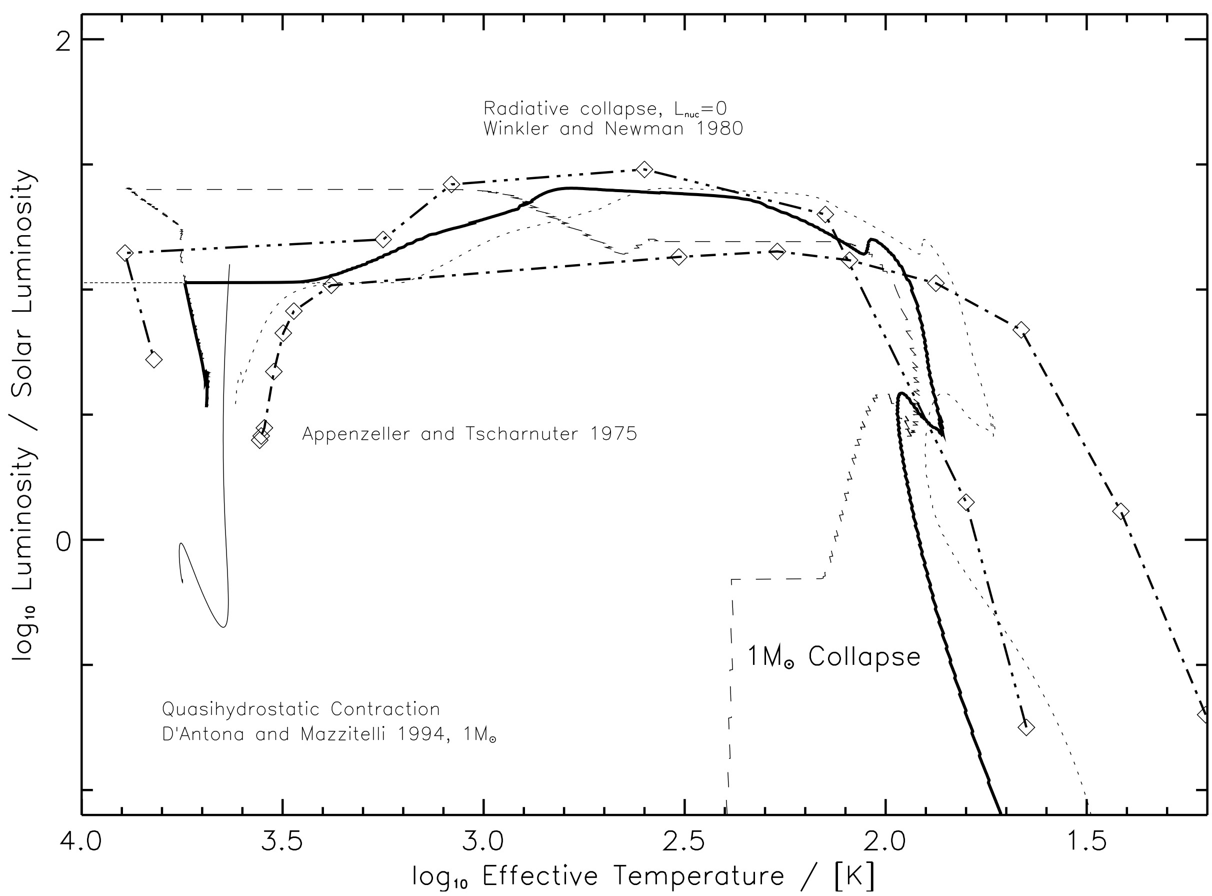

Fig. 6. Comparison of the results for the collapse of $1\,\mathrm{M}_\odot$, by Appenzeller and Tscharnuter (1975), *dash-dotted line*, and Winkler and Newman (1980a,b), *dash-triple-dotted line*, and a classical DM94, pre-main sequence track, *thin line*, and the collapse of a Bonnor-Ebert sphere (*thick line*, this work). The Winkler and Newman track is radiative, Appenzeller and Tscharnuter use ZEG-convection, the DM94-track and the track from this work are both calculated for mixing length convection, with $\alpha_{\rm ML} = 1.4$. The *thick line* for the cloud collapse gives the effective temperature, the *dashed line* is the temperature at the *temperature radius*, and the *dotted line* gives the photospheric temperature.

7.2. On the verge of the birthline

The birthline is a theoretical concept for obtaining a mass-radius relationship for young stars. It was introduced (Stahler 1988) as a correction to the concept of a Deuterium main sequence (Grossman and Graboske 1971) after $1\,\mathrm{M}_\odot$ collapse calculations had shown that stellar radii at pre-main sequence arrival had been overestimated by an order of magnitude (Larson 1969, Appenzeller and Tscharnuter 1975, Winkler and Newman 1980a,b Stahler Shu and Taam 1980a,b). By intersecting the mass-radius relationship with the evolutionary tracks of detailed fully hydrostatic PMS calculations, positions in the Hertzsprung Russell diagram that correspond to the mass-radius relations that depend on parameterized accretion are obtained. Stahler (1988) and Palla and Stahler (1990) developed mass-radius relations for low and intermediate mass stars respectively that are based on the thermostatic effect of D burning. Nuclear energy production in conjunction with convection was argued to stabilize stellar interior entropy at a constant value for a certain time. Hence the young stars would remain in the vicinity of the birthline for a longer period then above it. The birthline locations are indicated by the hatched areas in Fig. 7. The vertically hatched area gives the birthline for the same D abundance as used in this work and assumed mass accretion rates of 10^{-5} to $2\,10^{-6}\,\mathrm{M}_\odot/\mathrm{yr}$. The dotted area below corresponds to the respective locations in the HRD for zero D abundance. This is more relevant to our work since almost all D has been burnt before pre-main sequence arrival and D energy generation contributes less than 10% of the luminosity for $\log_{10} T_{\rm eff} > 3.4$ in our collapse calculation. In Stahler's analysis the D burning changes the squarish region into the bow-tie shaped one that corresponds to the birthlines for the mentioned range of mass-accretion rates. Following the birthline analysis one might expect the Appenzeller and Tscharnuter 1975 track to slow down if D

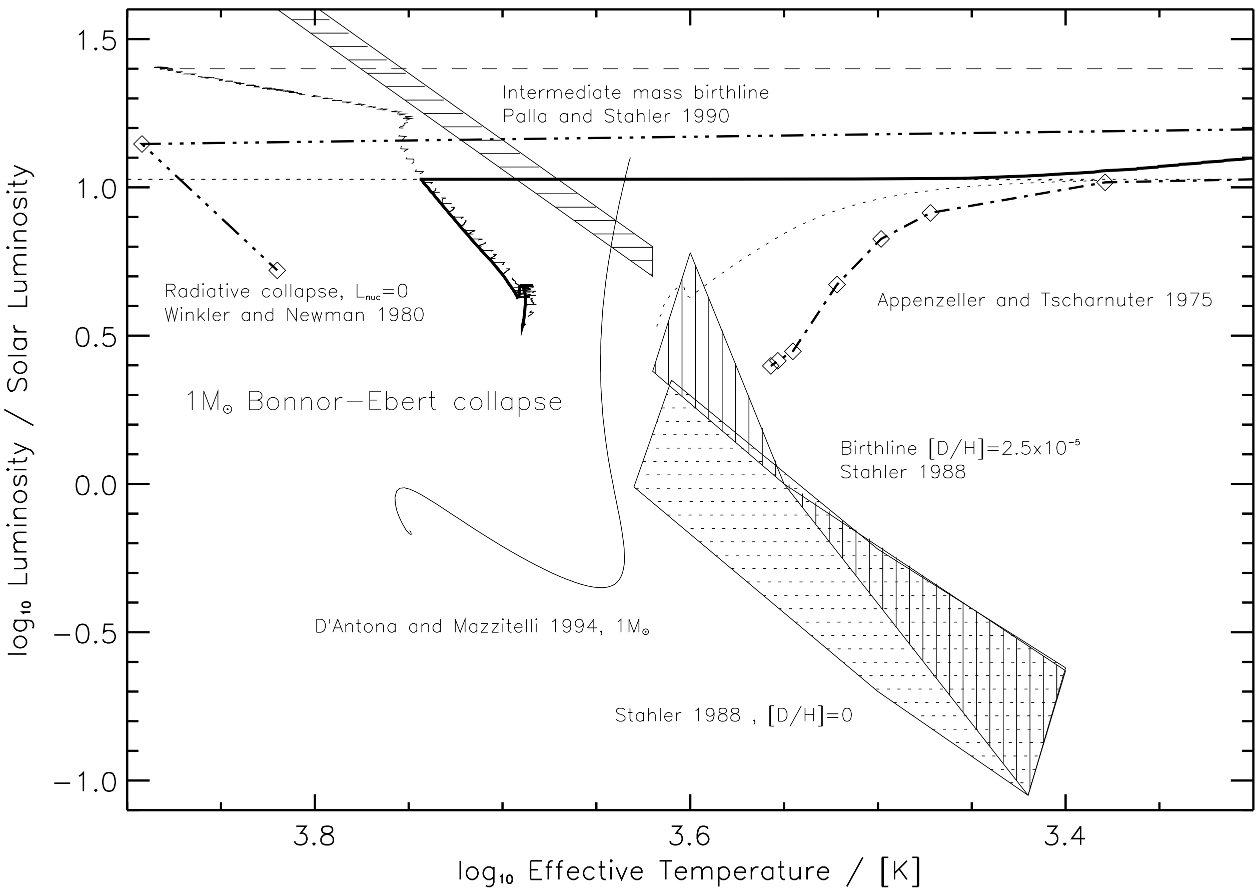

Fig. 7. Comparison of birthlines, collapse and fully hydrostatic pre-main sequence calculations. The low-mass birthline region for assumed mass-accretion rates between 10^{-5} and $2\,10^{-6}$ $M_\odot$/yr for a Deuterium number abundance ratio of $2.5\,10^{-5}$, from Stahler (1988), (*vertically hatched area*). This D abundance corresponds to D mass-fraction $X_{\rm D} = 3.85\,10^{-5}$, used in this work. The *dotted squarish region* is the respective area for zero D abundance. An estimate for the lower part of the intermediate mass birth line (from Palla and Stahler 1990) is shown as the *horizontally hatched* area. The collapse of a 'Bonnor-Ebert' sphere (*thick line*) and a classical pre-main sequence track (*thin line*) are both for mixing length convection, with $\alpha_{\rm ML} = 1.4$. The *thick line* for the cloud collapse gives the effective temperature, the *dashed line* is the temperature at the *temperature radius*, and the *dash-dotted line* gives the photospheric temperature. Collapse results from Appenzeller and Tscharnuter (1975) and Winkler and Newman (1980a) are depicted as the *dash-dotted* and *dash-triple-dotted* lines, respectively.

burning would start roughly at the end of the track. That the Appenzeller and Tscharnuter ZEG-track ends close to the birthline may not be a coincidence since the birthline heavily draws from the ZEG assumption and uses the constancy of entropy in the young stars interior for the development of the mass-radius relation. Due to the ZEG-convection assumption the interior structure should closely correspond to Stahler assumptions if the star would be fully convective. Winkler and Newman pointed out that due to the thermal profile produced by the collapse exhibiting an off-centre temperature maximum, the young star would presumably not be fully convective and might ignite D already at temperatures of 3–5 10^5 K and off centre. Our calculation confirms that suggestion. D burning starts at the bottom of a convective shell during the main accretion phase and does not render the protostellar core fully convective. In the interior there remains a radiative core that extends to about 20% of the radius at the end of the calculation. Accordingly our pre-main sequence track for 1 $M_\odot$ is located to the left of the Hayashi part of the fully hydrostatic DM94-track, and the birthline region relevant for a solar mass. It appears somewhat below the lower part of the Palla and Stahler (1990) birthline for intermediate masses and moves in a direction that first is initially almost parallel to the accreting radiative Winkler and Norman collapse track and after accretion luminosity has become insignificant turns in a direction pointing towards the ZAMS position of the Sun. Together with the fact that there is a radiative core in the interior this direction may be viewed as a mixture of Hayashi and Henyey track. This interpretation is corroborated by the fact the the direction is intermediate between the ZEG-convective Appenzeller and Tscharnuter collapse track and the radiative Winkler and Newman collapse calculation.

Finally we note that at the end of our Bonnor-Ebert collapse calculation the off-centre temperature maximum has reached $3\,10^6\,\mathrm{K}$ and hydrogen burning will slowly start, and also off-centre.

8. Conclusions

A study with spherical symmetry can certainly not address all aspects of the star formation process, as magnetic fields and angular momentum are ingnored, but it has the advantage that the process can be studied by keeping close to basic physical principles—at least as close as stellar evolution theory, with the notorious problem of the convection model.

Based on the concept of 'maximum deduction at minimum assumptions', spherical symmetry provides a useful limiting and reference case. With the symmetry assumption we were able to keep in close and explicit relation to the fundamental conservation laws and other basic physical principles. The essential modeling assumption that then goes into this work is the ever present problem of the convection model. But we have tried not to add ambiguity that is not already present in the modeling of stellar evolution. As a consequence of the convection model we use, our system of equations represents the Sun correctly. The number of free parameters in any study of star formation will not be made smaller than in ours unless there will be a parameter free description of convection.

The energetics of the star formation process can be addressed rather completely, most notably because all relevant energy transfer processes, i.e., radiation, convection, advection and conduction can be described accurately. Very likely star formation is most efficient with zero angular momentum and hence a lower limit for star formation time and upper limits for luminositites and accretion-rates are obtained.

In particular spherical collapse provides a well defined concept to provide initial conditions for stellar evolution, a necessity also for studies of coupled star/parameterized disk-accretion. It makes quantitative predictions for 'stellar' properties for the entire accretion process starting with the formation of a photosphere—when a radiating outer layer forms around an optically thick central cloud region—to the quasi-hydrostatic pre-main sequence contraction. We have shown that properties of stars with 'initial thermal structures' that result from the collapse of cloud fragments differ from those obtained with simplifying assumptions like isentropic or polytropic radial structure, that are commonly used as a starting point for the calculation of early stellar evolution (e.g. D'Antona and Mazzitelli 1994, Forestini 1994 (polytrope), Siess et al. 1997, 1999 (polytrope), Palla and Stahler 1991,1993 (fully convective, found $n = 3/2$ insufficient)).

With our assumptions we can describe the pre-main sequence evolution as a consequence of the star formation process, more precisely as a result of the collapse of Bonnor-Ebert spheres. The results of our study can be summarized in a Hertzsprung-Russell diagram, see Fig. 8, that shows the entire evolution from stellar zero age to the pre-main sequence. The accretion history of young stars of masses 2, 1, 0.5 and $0.1\,\mathrm{M}_\odot$ and a brown dwarf of $0.05\,\mathrm{M}_\odot$ show that the question of where a young object arrives on its pre-main sequence track depends on collapse flow and the cloud fragment mass. All 'stellar' masses appear at locations in the HRD that are different from the ones predicted by classical, fully hydrostatic calculations. In particular they do not start at the top of a classical, initially fully convective track or at the birthline. Those differences cannot be attributed to differences in energy transfer treatment or differences in microphysics since we have constructed our model equations in a way that assures a 'stellar structure' limit, that is approached during pre-main sequence contraction and that coincides with the assumptions made in our classical fully hydrostatic reference-study.

The ages obtained with collapse models differ significantly, i.e., up to 1 Myr, from the ages derived from classical calculations. This is only in part due to the fact that the time needed for collapse and accretion are not accounted for in classical PMS calculations. The primary reason is that the contraction behaviour of the young stars resulting from the collapse differs from the one obtained for the usually assumed fully convective, isentropic, or polytropic initial structures. The fact that Deuterium is almost completely burnt during the main accretion phase, i.e., before the PMS is reached for all 'truly' stellar masses calculated here (the $0.1\,\mathrm{M}_\odot$ case is the exception) also contributes to the difference. Hence calculations of early stellar evolution *depend* on the star formation process. Initial conditions are not forgotten in general. Another way to summarize this is that the star formation time, in our study about 3–4 free-fall times in all cases, is not sufficiently different from the Kelvin-Helmholtz time-scale of young objects to separate initial energy deposition into the star during the accretion phase from energy losses that controll the contraction to the main sequence. As a consequence, protostellar collapse determines the PMS evolution.

This effect is enhanced by the off-centre ingnition of D burning and its interaction with the thermal structure. Unlike during most of stellar evolution it is not only controlled by the existing thermal structure but helps also to conserve the global thermal structure *outside* thermal equilibrium. This differs from the usual behaviour close to complete equilibrium, e.g., of main sequence stars, where

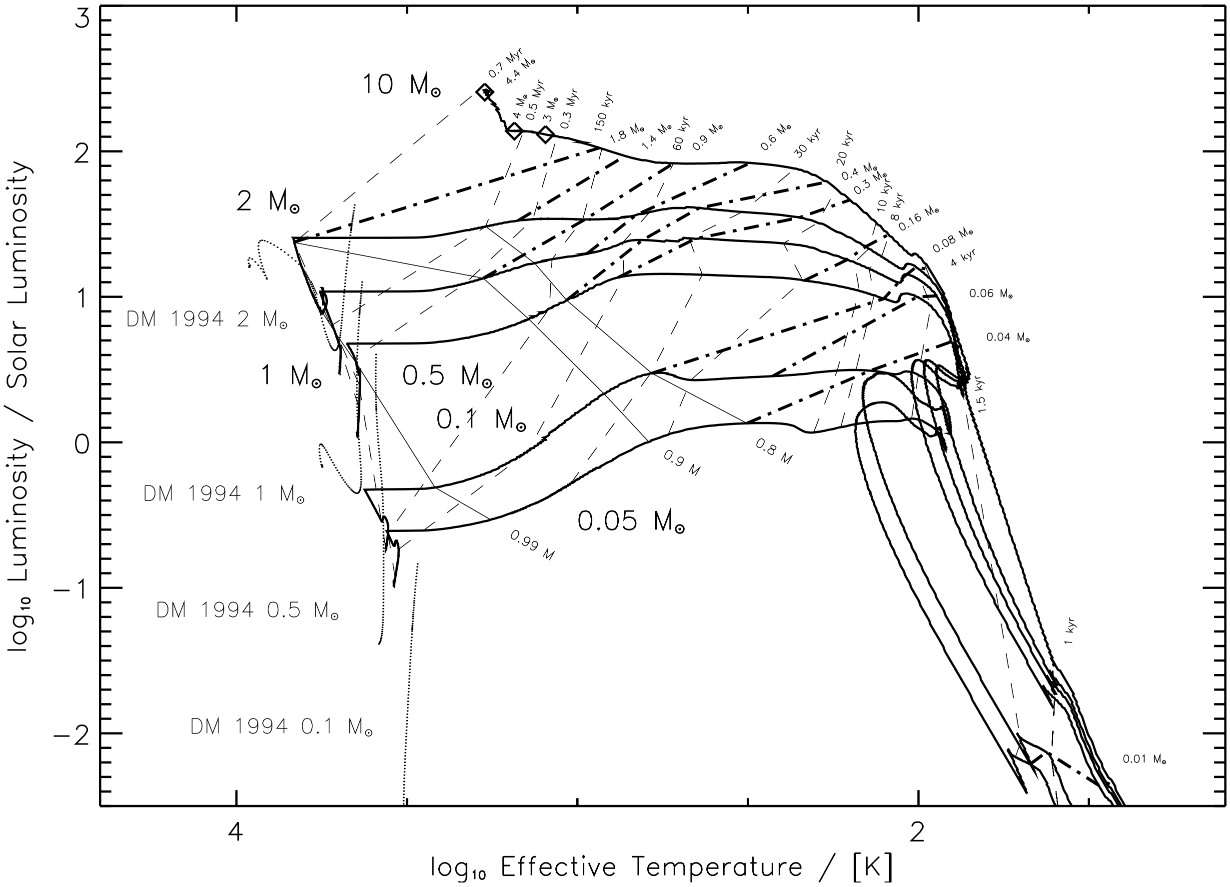

Fig. 8. A summary of the pre-main sequence evolution resulting from the collapse of 10 K Bonnor-Ebert spheres. Results are shown for cloud-fragments of 0.05, 0.1, 0.5, 1, 2 and 10 $\mathrm{M}_\odot$. *Thick lines* are evolutionary tracks, *dashed lines* are isochrones, *dash-dotted lines* are isopleths for optically thick mass, M_τ. Isochrones and isopleths are labelled along the 10 $\mathrm{M}_\odot$-track. The locations where M_τ corresponds to 80, 90 and 99% of the final mass are connected by the *thin lines*. Quasi-hydrostatic tracks for $0.1, 0.5, 1$ and $2\,\mathrm{M}_\odot$ are shown as *dotted lines* for comparison.

nuclear reactions are adjusted to the thermal needs of the star and re-establish global thermal equilibrium.

Our study re-emphasizes the fact that star formation is an intrinsically time dependent process, with variations in all flow quantities. We have tried to tentatively group the young population into four different evolutionary phases based on the fraction of the residual circumstellar mass around them. We gave characteristic quantities for those phases showing that mass accretion rates vary significantly over the main accretion phase. Accretion rates are typically a few $10^{-6}\,\mathrm{M}_\odot/\mathrm{yr}$ in the earliest phase, a few $10^{-7}\,\mathrm{M}_\odot/\mathrm{yr}$ for the last 10% and a few $10^{-8}\,\mathrm{M}_\odot/\mathrm{yr}$ for the accretion of the last percent of the final mass. Those values are not too far from what is currently inferred from observations (e.g., Brown and Chandler 1999). Also our star formation times of 0.07 to 1.3 Myr for 0.1 to 2 $\mathrm{M}_\odot$ are consistent with estimates from a comparison of T-Tauri star- and embedded source counts (Kenyon et. al. 1990). Our median luminosities between about 0.3 to 10 $\mathrm{L}_\odot$, depending on accretion phases, for cloud fragment masses from 0.01 to 0.5 $\mathrm{M}_\odot$, make it much harder to construct a 'Class I luminosity problem' than with the assumed constant, canonical mass accretion rate of $10^{-5}\,\mathrm{M}_\odot/\mathrm{yr}$, that is in conflict with observations (Brown and Chandler 1999).

Let us finally summarize our main points:

- the star formation processes, i.e., the protostellar collapse translates initial cloud conditions into initial stellar thermal structure,
- pre-main sequence evolution depends qualitatively and quantitatively on the collapse flows;
- D burning ignites and mostly occurs during the accretion phase for cloud fragments of 0.5, 1, 2, and 10 $\mathrm{M}_\odot$;
- we confirm that protostars and PMS objects have an outer convective shell and a central radiative zone;
- the radiative core lasts at least to a (new) age of 1.5 Myr for cloud fragments of 0.5, 1, and 2 $\mathrm{M}_\odot$ and we expect off-centre ignition of hydrogen burning;

– collapse pre-main sequence tracks are initially cooler than classical tracks. Later they *cross* the Hayashi line rapidly and start their quasi-classical decent along a mixed radiative/convective contraction track. After the final stellar photosphere becomes visible they appear to the left of the Hayashi lines. Typically at 0.05 dex hotter effective temperatures than the corresponding classical, fully hydrostatic pre-main sequence model;
– collapse ages below 2 Myr are up to a Myr larger than classical ages for the same luminosity.

Acknowledgements. This work is supported by the *Fonds zur Förderung der wissenschaftlichen Forschung (FWF)* under project numbers S7305–AST and S7307–AST and the *Deutsche Forschungsgemeinschaft (DFG)*, SFB 359 (key research project of the German national science foundation on 'Reactive flows, diffusion and transport'). GW thanks M. Feuchtinger for the collaboration on the convection model and sharing the version of the VIP-code and the computational environment that he developed. We thank E. Dorfi for developing and sharing the original version of the VIP-code and providing substantial amounts of computational resources on his VAX-cluster in Vienna where the computations were perfomed, and for comments and discussion. We thank Christian Straka for reading the manuscript. We are indepted to Prof. H. Petersmann (Seminar für Klassische Philologie der Univ. Heidelberg) for a most elucidated advice on the semantics and etymology of the term *isopleths.*

References

Alexander, D. R. and J. W. Ferguson 1994 Astrophys. Journ. **437**, 879
Allègre, C.J., Manhès, G., Göppel, C. 1995 Geochim. Cosmochim. Acta 59, 1445
Appenzeller, I. 1982 in Landolt-Börnstein, Zahlenwerte und Funktionen aus Naturwissenschaft und Technik, Neue Serie, Gruppe IV: Astronomie Astrophysik und Weltraumforschung, Bd. 2, Astronomie und Astrophysik, Teilband b, Sterne und Sternhaufen, (Schaifers, K. Voigt, H.H. eds.), pp. 357 Springer, Berlin 1982.
Appenzeller, I., Tscharnuter, W. 1974, A&A 30, 423
Appenzeller, I., Tscharnuter, W. 1975, A&A 40, 397
Balluch, M., 1991a, A&A 243, 168
Balluch, M., 1991b, A&A 243, 187
Balluch, M., 1991c, A&A 243, 205
Baschek, B., Scholz, M., Wehrse R., 1991, A&A 246, 374
Bertout, C., 1976 A&A 51, 101
Brown, D.W., Chandler, C.J., 1999 MNRAS 303, 855
Castor, J.I., 1972, ApJ 178, 779
Chabrier, G., Baraffe, I., 1997, A&A 327, 1039
Caughlan, G.R., Fowler, W.A. 1988 *Atomic Data and Nuclear Data Tables*, **40**, 283–334
D'Antona, F. and Mazzitelli, I. (1994) New Pre-Main-Sequence Tracks for $M \leq 2.5 M_\odot$ As Tests of Opacities and Convection Model. Astrophys. Journ. Suppl. Ser. bf 90, 457–500
Dorfi, E.A, 1998 in *Computational Methods for Astrophysical Fluid Flow*, (Steiner, O. and Gautschy, A. eds.) Springer 1998
Dorfi, E.A., Drury, L.O'C., 1987, J. Comp. Phys. 69, 175
Dorfi, E.A., Feuchtinger, M.U., 1995 Comp. Phys. Comm. 89, 69–90
Dorfi, E.A., Feuchtinger, M.U., 1999, A&A, submitted.
Feuchtinger, M.U., 1998a, A&A 337, L31
Feuchtinger, M.U., 1999a A&A Suppl. 136, 217
Feuchtinger, M.U., 1999b, A&A submitted.
Feuchtinger, M.U., Dorfi, E.A., 1994, A&A 291, 225
Feuchtinger, M.U., Dorfi, E.A., 1997, in *A half century of stellar pulsations*, Ed. J.A. Guzik, Los Alamos 1997, ASP Conference Series
Feuchtinger, M.U., Dorfi, E.A., 1999, A&A submitted
Forestini, M., 1994, A&A 285, 473
Foster, N.P., Chevalier, R.A. 1993, ApJ 416, 303
Grossmann A.S., Graboske, H.C. 1971 ApJ 164, 475
Gehmeyr, M., Mihalas, D. 1993 American Astronomical Society Meeting, 183, #48.06 (abstract) http://141.142.3.131/Pubs/TechReports/TechReportsSeries.html
Hayashi, C., Hoshi, R., Sugimoto, D. 1962, Prog. Theor. Phys. 22, Suppl., pp. 174–176
Götz, M. 1993. Dissertation, Univ. Heidelberg.
Kenyon, S.J., Hartmann, L.W., Strom, K.M., Strom, S.E. 1990 AJ 99, 896
Kippenhahn, R., Weigert, A., 1990, Stellar Structure and Evolution, p. 42, Springer, Berlin
Kuhfuß, R., 1986, A&A 160, 116
Kuhfuß, R., 1987, 'Ein Modell für zeitabhängige Konvektion in Sternen', PhD-Thesis, TU München
Kürschner, R. 1994 A&A 285, 897
Larson, R.B. 1969 MNRAS 145, 271
Lenzuni, P., Chernoff, D.F., Salpeter, E.E. 1992, Ap.J. 393, 232
LeVeque, R., 1998 in *Computational Methods for Astrophysical Fluid Flow*, (Steiner, O. and Gautschy, A. eds.) Springer 1998
Mihalas, D., Däppen, W., Hummer, D.G. 1988 Ap.J. 331, 815
Mihalas, D., Mihalas, B.W.: 1984, *Foundatios of Radiation Hydrodynamics,* Oxford University Press, New York
Mihalas, D. 1998 in *Computational Methods for Astrophysical Fluid Flow*, (Steiner, O. and Gautschy, A. eds.) Springer 1998
Morfill, G., Tscharnuter, W.M., Völk, H. 1985 In *Protostars and Planets II*, eds. D. C. Black and M. S. Matthews, Tucson: Univ. of Arizona Press, pp. 493
PPII
Ondrejkovics-Fernandes, M.G. 1990. Dissertation, Univ. Wien.
Palla,F. and Stahler,S.W. 1990 ApJ 360,L47
Palla,F. and Stahler,S.W. 1991 ApJ 375,288
Palla,F. and Stahler,S.W. 1992 ApJ 392,667
Siess, L., Forestini, M., Bertout, C. 1997, A&A 326, 1001
Siess, L., Forestini, M., Bertout, C. 1999, A&A 342, 480.
Stahler, S.W. 1988 ApJ 332, 804
Stahler, S.W. Shu, F.H., Taam, R.E. 1980a ApJ 241, 637
Stahler, S.W. Shu, F.H., Taam, R.E. 1980b ApJ 242, 226
Stahler, S.W. Shu, F.H., Taam, R.E. 1981 ApJ 248, 727
Tscharnuter, W.M. 1987, A&A 188, 55
Tscharnuter, W.M. 1989, in Proceedings of the ESO Workshop on Low Mass Star Formation and Pre-main Sequence Objects, held in Garching bei Munchen, F.R.G., July 11-13, 1989. Editor, Bo Reipurth; Publisher, European Southern Observatory, Garching bei Munchen,

Equations for protostellar collapse and pre-main sequence evolution

$$\Delta M_r = \int_{V(t)} \varrho \, d\tau$$

$$\frac{d}{dt}\left[\int_{V(t)} \varrho \, d\tau\right] + \int_{\partial V} \varrho(u_{\rm rel} \cdot dS) = 0$$

$$\frac{d}{dt}\left[\int_{V(t)} \varrho_D \, d\tau\right] + \int_{\partial V} [\varrho_D u_{\rm rel} + j_{\rm D}] \cdot dS = \int_{V(t)} \dot{\varrho}_D \, d\tau$$

$$\frac{d}{dt}\left[\int_{V(t)} \varrho u \, d\tau\right] + \int_{\partial V} \varrho u(u_{\rm rel} \cdot dS) + \int_V \left(\frac{\partial p}{\partial r} + \varrho \frac{GM_r}{r^2}\right) d\tau = C_M$$

$$\frac{d}{dt}\left[\int_{V(t)} \varrho(e+\omega) \, d\tau\right] + \int_{\partial V} [\varrho(e+\omega)u_{\rm rel} + j_w] \cdot dS + \int_V p \, {\rm div}\, u \, d\tau = -C_E + \int_{V(t)} \varrho \epsilon^D_{\rm nuc} \, d\tau$$

$$\frac{d}{dt}\left[\int_{V(t)} E \, d\tau\right] + \int_{\partial V} [E u_{\rm rel} + F] \cdot dS + \int_V P \, {\rm div}\, u \, d\tau = C_E$$

$$\frac{d}{dt}\left[\int_{V(t)} \frac{F}{c^2} \, d\tau\right] + \int_{\partial V} \frac{F}{c^2}(u_{\rm rel} \cdot dS) + \int_V \left(\frac{\partial P}{\partial r} + \frac{F}{c^2}\frac{\partial u}{\partial r}\right) d\tau = -C_M$$

$$\frac{d}{dt}\left[\int_{V(t)} \varrho\omega \, d\tau\right] + \int_{\partial V} \varrho\omega u_{\rm rel} \cdot dS = \int_{V(t)} \left(S_\omega - \tilde{S}_\omega - D_{\rm rad}\right) d\tau$$

$$C_M = \int_V \kappa\varrho \frac{F}{c} \, d\tau \,, \quad C_E = \int_V \kappa\varrho(4\pi S - cE) d\tau$$
$$S_\omega = -\nabla_{\rm s} \frac{T}{P}\frac{\partial P}{\partial r}\Pi \quad \Pi \propto -\frac{\partial s}{\partial r} = \frac{c_p}{H_p}(\nabla - \nabla_{\rm s}) \tag{30}$$

Table 1. The equations are applied to spherical volumes. Note that the expression for convective Source term, S_ω , that contains the Schwarzschild-Ledoux criterion. Convectively unstable stratifications occur in the present terminology and with spherical symmetry when pressure and temperature gradients have the same sign and produce a positive value of S_ω that then contributes a source of turbulent kinetic energy, $\omega = 3/2 u_c^2$ in the balance equation of turbulent kinetic energy. Note that S_ω can also act as a sink, corresponding to damping of convection due to damping bouyancy effects — a property not usually assured in convection models. Note that the expression given in Equ. (5) of Wuchterl and Feuchtinger (1998) gives the wrong sign for S_ω.

Boundary Conditions

At the outer boundary the moment equations of the RTE are closed by

$$J = B(T_{\rm ext}) + \frac{1}{\bar{\mu}} H \tag{31}$$

with $T_{\rm ext} = 10\,{\rm K}$ and $\bar{\mu} = 1/2$ (Yorke 1980b). I.e., radiation is streaming freely into an external reservoir emitting blackbody radiation of 10 K. All other surface terms vanish both at the outer cloud boundary (e.g., no convective flux leaves the fragment) and at the centre, where the interior mass M_r is zero. The total volume of the computed domain is assumed to be constant, equal to the volume of the critical Bonnor-Ebert sphere.

Tscharnuter, W.M. 1991 in *The Physics of Star Formation and Early Stellar Evolution* (Lada, C.D. and Kylafis, N.D. eds.) NATO ASI, Series C Vol. 342 pp. 411–436 Kluwer Dordrecht 1991

bibitem Tscharnuter, W.M., Boss, A.P. 1993 In *Protostars & Planets III*, eds. E. H. Levy and J. I. Lunine Tucson: Univ. of Arizona Press), pp. 367

Tscharnuter, W.M. and Winkler, K.-H.,A. 1979 Comp. Phys. Comm. 80, 171

Weiss, A., Keady, J.J., Magee, N.H.,Jr. 1990 Atomic Data and Nuclear Data Tables 45, 209
Winkler, K.-H.A. and Newman, M.J. 1980a ApJ 236, 201
Winkler, K.-H.A. and Newman, M.J. 1980b ApJ 238, 311
Wuchterl, G., 1990, A&A 238, 831992
Wuchterl, G., 1995a , Comp. Phys. Comm. 89, 119
Wuchterl, G., 1995b, Earth, Moon and Planets 67, 51
Wuchterl, G. and Feuchtinger M.U. 1998 Astron. Astrophys. **340**, 419–430
Yorke, H.W., 1979, A&A 80, 308
Yorke, H.W., 1980a, A&A 85, 215
Yorke, H.W., 1980b , A&A 86, 286